

Pipe Routing with Topology Control for UAV Networks

Shreyas Devaraju, *Student Member, IEEE*, Shivam Garg, *Member, IEEE*, Alexander Ihler, *Member, IEEE*, Sunil Kumar, *Senior Member, IEEE*

Abstract—Routing protocols help in transmitting the sensed data from UAVs monitoring the targets (called target UAVs) to the BS. However, the highly dynamic nature of an autonomous, decentralized UAV network leads to frequent route breaks or traffic disruptions. Traditional routing schemes cannot quickly adapt to dynamic UAV networks and/or incur large control overhead and delays. To establish stable, high-quality routes from target UAVs to the BS, we design a hybrid reactive routing scheme called pipe routing that is mobility, congestion, and energy-aware. The pipe routing scheme discovers routes on-demand and proactively switches to alternate high-quality routes within a limited region around the active routes (called the pipe) when needed, reducing the number of route breaks and increasing data throughput. We then design a novel topology control-based pipe routing scheme to maintain robust connectivity in the pipe region around the active routes, leading to improved route stability and increased throughput with minimal impact on the coverage performance of the UAV network.

Index Terms—Unmanned aerial vehicles, autonomous UAV networks, routing, topology control, mobility model, network connectivity.

I. INTRODUCTION

Unmanned aerial vehicles (UAVs) equipped with self-localization and sensing capabilities have become popular for applications such as area monitoring, surveillance, search-and-rescue, and target tracking [1]–[3]. We focus on low SWaP (size, weight, and power), fixed-wing UAVs, which offer a balance of portability and area coverage (with higher speeds and longer lifetimes than rotor-based UAVs). However, low SWaP UAVs face some practical difficulties: they have limited communication range and are more prone to failure than larger UAVs. These issues motivate a **decentralized** and **autonomous** network of UAVs, in which the nodes explore an area, perform local sensing, and communicate with their neighbors without any global knowledge of network topology.

We consider a network of low SWaP fixed-wing UAVs deployed in an area without any fixed communication infrastructure, such as a cellular network. Example targets might be buildings on fire or a damaged bridge in a disaster area, or enemy troop movements on a battlefield, so the targets need constant monitoring. When one or more targets of interest are

found, a UAV (called the *target UAV*) continuously monitors each target and transmits the sensed information back to the base station (BS) in real time. The remaining UAVs continue to collaboratively monitor the area to find new targets while maintaining connectivity and communication routes to the BS.

The goal of a routing protocol is to help establish communication routes along which the sensed data can be transmitted from each target UAV to the BS. However, the highly dynamic nature of an autonomous decentralized UAV network can result in frequent changes in the network topology, causing existing routes to break or creating traffic disruptions. The disrupted network may experience loss of data (packet drops), increased control and computational overhead, as more resources are devoted to the frequent route rediscoveries, and corresponding increased delays in the transmission of the target data. Most existing routing schemes cannot update the routing table or discover a new route before the current route breaks. *Reactive* routing schemes then create significant delays, since they perform new route discovery while the current routes are broken. On the other hand, *proactive* routing schemes introduce large overheads, as each node periodically transmits control messages to maintain and update the routes in the network [4]. Another concern in our application, in which all the target UAVs need to relay their information to a single base station, is that the routes may converge and create high resource usage (and congestion) at nodes along any shared routes, especially at high data rates. These “hot-spot” nodes along shared routes can become critical points of failure, causing communication disruptions. Low SWaP UAVs have limited battery capacity, and their residual energy levels may vary depending on usage (flight duration and trajectories). Selecting UAVs with low energy reserves to participate in routes to the BS inevitably results in disruption of the data flows when these low-energy UAVs fail.

To mitigate these issues, a good routing protocol should be mobility, congestion, and energy-aware. We say a routing protocol is “mobility-aware” if its selection of routes in a network is based on the trajectories of nodes within the route; it can select long-lasting routes by considering the estimated lifespan of a chosen route [5]–[7]. “Congestion-aware” routing protocols select routes that minimize congestion by avoiding congested nodes [4], [8]–[11]. Finally, “energy-aware” routing involves selecting nodes above a minimum energy level required to provide stable and long-lasting routes.

Of course, the ability of a routing protocol to find or switch routes depends on the availability of routes between the source and destination. Hence, routing protocols alone cannot

S. Devaraju is with Computational Science Research Center, San Diego State University & University of California, Irvine, USA, sdevaraju@sdsu.edu

S. Garg is with Electrical & Computer Engineering Department, San Diego State University, San Diego, California, USA, sgarg@sdsu.edu

A. Ihler is with School of Information & Computer Science, University of California, Irvine, USA, ihler@ics.uci.edu

S. Kumar is with Electrical & Computer Engineering Department, San Diego State University, San Diego, California, USA, skumar@sdsu.edu

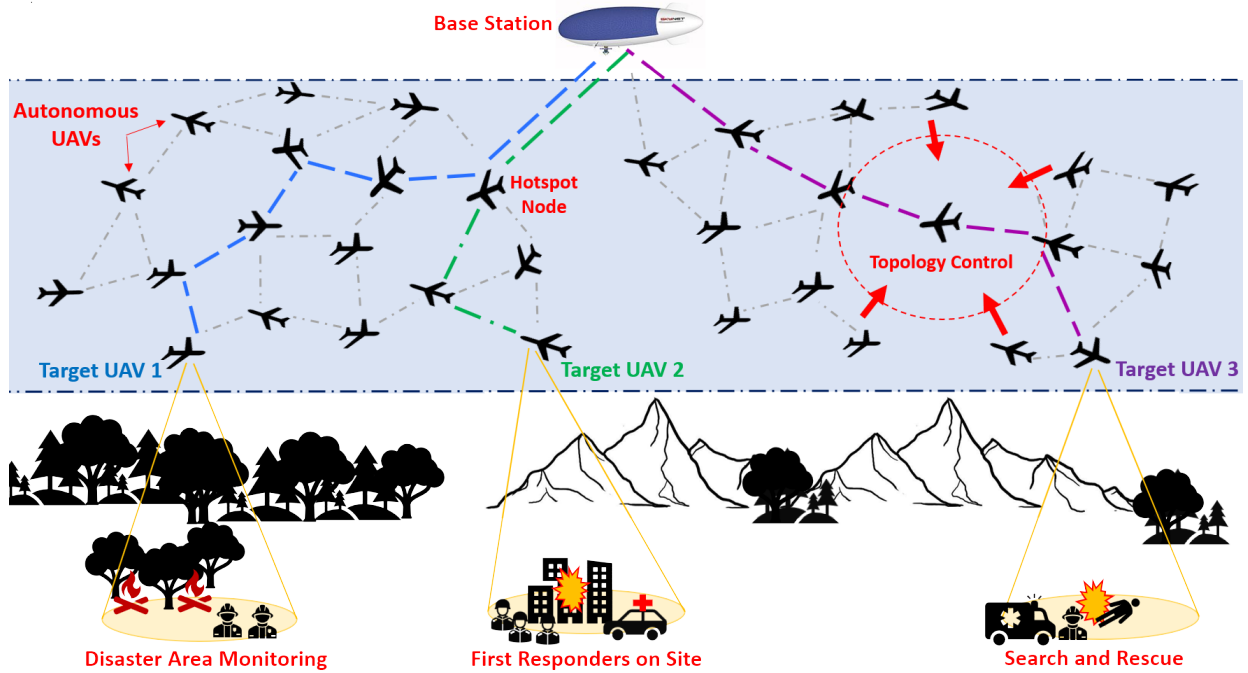


Fig. 1: Decentralized, autonomous UAV network performing monitoring, search and surveillance in inaccessible disaster areas.

guarantee the stability and quality of the routes; the nodes' mobility model plays a crucial role. For this reason, we use the BS-CAP mobility [12], a pheromone-based connectivity-aware mobility model, to improve overall network and BS connectivity. Our focus is on enhancing the stability and quality of routes between target UAVs and the BS; to this end, we propose a pheromone-based topology control mechanism to increase the density of UAVs around an active route. This improves the availability of high-quality routes and enables the routing protocol to choose the best route (long-lasting and less congested) from the available options.

We build our approach on a hybrid reactive routing protocol called MCA-AODV [13], and design a novel energy-aware routing protocol, called **Pipe routing**, as well as a complementary topology control scheme, together called **TC-Pipe routing**. These schemes select a stable route between each target UAV and the BS, while also considering the energy level of the nodes along the selected route. A relay based routing scheme is also discussed for comparison against the performance of both pipe based routing schemes.

- We design a mobility, congestion, and energy-aware hybrid reactive routing protocol, called **Pipe routing**, by modifying the MCA-AODV [13] routing protocol. This routing protocol is able to adapt to highly dynamic UAV networks and proactively switch or select stable and high-quality routes.
- Energy awareness prevents the selection of routes with low-energy UAVs; this avoids disruption of the data flows when these low-energy UAVs fail.
- Congestion-aware routes reduce the congestion at hotspot nodes when multiple flows to the BS are present in the network (especially at high data rates).
- A novel pheromone-based topology control scheme is

designed; it works in conjunction with the Pipe routing scheme, and is called **TC-Pipe routing**. The TC-Pipe scheme improves the availability of high-quality routes between the target UAVs and BS.

- The TC-Pipe routing scheme maintains robust connectivity around the active routes, leading to improved route stability and increased throughput with minimal impact on the coverage performance of the UAV network.
- Both the TC-Pipe and Pipe schemes' PDR and coverage performance decrease gracefully in proportion to the % UAVs failing in the network.
- A relay based routing scheme that uses dedicated relay nodes is also discussed for comparison against the performance of the Pipe and TC-Pipe routing schemes

Paper Organization: We first review several existing routing and topology control schemes that focus on providing robust routes (Section II). Next, we discuss our proposed pipe routing and topology control schemes in Sections III and IV, respectively, followed by the relay based routing scheme in Section VI. We evaluate the performance of our approach in simulations and analyze the results in Section VII.

II. RELATED WORK

Designing a resilient, robust routing protocol for autonomous, decentralized UAV networks is challenging: the network topology is highly dynamic, and traffic undergoes frequent fluctuations [11], [14]–[16]. Proactive routing schemes, such as OLSR and its variants [4], [17], introduce large control and computational overhead [4] and may increase congestion in the network.

On the other hand, reactive routing schemes [16], [18]–[27] discover new routes only on demand, and thus incur lower control and computational overhead. However, reactive methods

create higher route discovery delays. Route re-discovery can be especially problematic when routes break frequently, as in a dynamic UAV network. Many reactive routing schemes [15], [18] suffer from control packet (RREQ) flooding problems, known as “broadcast storms” [16]. Although some schemes [16], [21], [22] explicitly try to reduce the overhead and delay caused by frequent route discoveries, this often comes at the cost of using the best information. For example, in [22], when a route breaks, the intermediate nodes search for an alternate route only in their respective k -hop neighborhood; this reduces control overhead by avoiding network-wide route discovery by the source node. In [21], RREQ flooding is limited by only forwarding the RREQ to certain nodes identified in different zones based on the neighboring nodes’ location and connectivity. However, since the full network topology is not used for route discovery, these schemes can result in the selection of poor routes.

Many applications are time sensitive (e.g., video streaming) and demand a certain bandwidth level from the network. Reactive routing schemes that are QoS-aware [13], [23], [24], [28] use network statistics such as node mobility, link stability, hop count, signal strength, node energy level, congestion, and traffic load to select the best route. In one such scheme [23], RREQ is rebroadcast by only those nodes that meet specific QoS thresholds like time-to-live (TTL), bandwidth, and flow jitter. However, this protocol does not estimate or track node mobility and link stability, leading to frequent route breaks. In [24], an intermediate node in the route can adapt to the changes in the network topology and traffic conditions by selecting a new downstream node (towards the destination). This selection is based on neighbor distance, latency, traffic load, and reliability. However, this scheme can sometimes result in longer and less efficient routes. An energy-aware variant of AODV [28] uses the link stability and residual energy of the nodes to select stable routes.

Multipath reactive routing protocols [20], [25] find multiple node-disjoint or link-disjoint paths during route discovery and cache them as backup routes. When the current route quality degrades, the backup routes from the cache are used instead of performing a new route discovery. However, like the current route, the quality of the backup routes also typically decline over time. To avoid selecting bad routes, [26], [27] periodically monitor the quality of the backup routes. Whereas [16] performs local route repair using route recovery messages and uses fuzzy logic route selection based on node mobility, residual energy, and link quality. Link stability based reactive routing protocol [19] uses a semi-proactive route switching mechanism, which reduces route discovery overhead incurred in [16], [26], [27]. Here, the intermediate nodes notify the destination node of the route whenever the quality of the link to their downstream nodes degrades. Then the destination node sends a new RREP packet (containing the updated route stability value) to the source node along each cached route. The source node then switches to an alternate route, which avoids the high overhead and delay of new route discovery. However, this scheme is unable to adjust to traffic changes and congestion and also lacks a route repair mechanism.

A scalable hybrid routing protocol called mobility and

congestion-aware AODV (MCA-AODV) [13] combines reactive and proactive routing methods to adapt to dynamic UAV networks with lower control overhead than traditional proactive networks. Here, the source node maintains knowledge of alternate routes and their quality within a 2-hop region around the selected route (called a “pipe”) to perform proactive route switching when the quality of the current route degrades. MCA-AODV is both mobility and congestion-aware. It selects the best route based on various factors such as hop count, interference, route lifetime, and estimated latency to provide long-lasting and less congested routes.

Topology Control for Robust Routes: Some schemes (e.g., [12], [29]–[33]) modify the mobility models to provide stable network connectivity. In this section, we review topology control and routing schemes that maintain a stable active route between the source and destination UAVs. In [34], the AODV routing protocol [18] and a modified Boids mobility model [35] are used to maintain the links over the route in a highly dynamic autonomous UAV network. In [36], a global joint 3D trajectory and power allocation scheme was designed using spectral graph theory and convex optimization techniques to form interference-aware routes between a single source and destination (BS) using rotary wing UAVs. In [37], a mobility control system for FANETs based on virtual springs maintains an aerial mesh network to ensure ground-user coverage and QoS for disaster recovery. In [38], a virtual force-based UAV mobility model and energy-efficient mobility-aware cluster head (CH) UAV selection is used to improve ground-user coverage and network connectivity. Authors also propose a topology-aware routing protocol that uses Q-learning to find stable, low-delay and energy-efficient routes between CH UAVs and BS.

Our proposed routing protocol for autonomous UAV networks combines the advantages of both proactive and reactive schemes, along with topology control, to establish robust and low-overhead routes that are also mobility, congestion and energy aware. This protocol is based on our connectivity-aware pheromone mobility model that balances maintaining connectivity with providing coverage [12].

A. Overview of UAV Mobility Models

Pheromone mobility models use digital repel pheromones to promote exploration and fast coverage of an area with no prior information [3], [30]. We consider a decentralized connectivity-aware pheromone-based UAV mobility such as BS-CAP [12] in our experiments, to provide fast area coverage, strong node degree, and base station connectivity. In BS-CAP, the UAVs move and deposit repel pheromones in virtual maps divided into grid cells, and the trajectory of a UAV (controlled by its next-waypoint) is decided based on the repel pheromone in cells and the node degree at a set of candidate waypoints, while ensuring that the next-waypoint maintains a route to the BS. The coverage and connectivity trade-off is controlled by adjusting the weight given to the UAVs’ node degree at the waypoints. In the sequel, we also modify the BS-CAP model to provide topology control in the pipe, and increase the density of UAVs around an active route (see Sections III and IV).

Another connectivity-aware UAV mobility model used in our experiments is the *ConCov model* [31], which uses a modified flocking behavior to provide trade-offs between coverage and BS connectivity. The ConCov model uses artificial potential fields, along with 1-hop neighbor locations and their routing information, to minimize overlap in the area sensed by neighboring UAVs but maintain BS connectivity. The heading of a UAV is the weighted sum of repelling forces from neighboring UAVs and an attractive force to a neighboring UAV with a route to the BS. The coverage/connectivity trade-off can be tuned by adjusting the relative weight of these two forces.

III. PIPE ROUTING SCHEME

The Pipe routing scheme selects and maintains a stable route between each target UAV and the BS, known as an *active route*. It is based on a mobility and congestion-aware, hybrid reactive routing scheme [13]. Since the UAVs participating on an active route also participate in area coverage and exploration tasks (e.g., following the BS-CAP mobility model [12]), the resulting network topology changes over time, which can cause link breaks and/or changes in route quality. Pipe routing proactively maintains the network information of a narrow, 2-hop region of nodes around the active route (called the “pipe”; see Section III-C), and the source node performs a “multi-metric” route selection (Sections III-A and III-B) to switch to a new, higher-quality route when required. Because it takes into account the node mobility, available energy, and congestion, the Pipe routing scheme selects less congested and long-lasting routes with fewer route breaks, while also incurring little route discovery overhead. When the quality of the current route drops below a pre-defined threshold, the source node proactively switches to a new route within the pipe without triggering a new route discovery.

A. Description of Routing Metrics

To choose a stable, low congestion route with a long lifetime, we use several route information metrics, capturing route length, interference, anticipated route lifetime, and available energy. In particular, we use the hop count (HC, the number of links between the target UAV and the BS) along with the total number of interfering links (IL) across all UAVs in the route. The route lifetime (RLT) is the estimated time duration after which the route is likely to break; it is the minimum estimated link lifetime (LLT) over all the links that form the route. A UAV estimates the LLT of a link with its neighbors using the GPS and current trajectory information found in the Hello message from its neighbors. Additional details on computing these metrics can be found in [13].

In addition to the given route metrics, the residual energy of the route (En_R) is computed as the minimum energy across all nodes in the route. If En_i is the energy level of node i in the route (R), and N_R is the set of nodes, then

$$En_R = \min_{i \in N_R} (En_i) \quad (1)$$

UAVs with energy levels below a threshold (En_{th}) are likely to run out of battery soon, resulting in node failure and causing

a route break. Therefore, these UAVs should safely disengage from the route. For this reason, routes with $En_R \leq En_{th} + \delta_e$ are not considered during route selection in our scheme. Since the source node receives updated topology information (node energy) every 2 s, we select the value of the tolerance factor δ_e to be twice the per-second energy depletion rate of a UAV to account for the delay. Moreover, preemptive route switching is performed when the currently active route’s En_R falls below the threshold En_{th} .

B. Active Route Selection

During the route discovery process, if the target UAV (source node) does not already have a route to the destination (in our setting, the BS), it broadcasts an RREQ message towards the BS. Unlike MCA-AODV [13], which floods RREQ messages in the entire network, our scheme takes advantage of the UAV’s knowledge about the BS’s GPS location and broadcasts the RREQ messages only in the direction of the BS. In response, the BS sends back RREP messages to the target UAV over the reverse routes, identified during the RREQ forwarding phase. To find stable routes, with a low control packet overhead, RREQ forwarding is limited to intermediate nodes that meet both the link stability condition (as in Eq. (1) of [13]) and the energy threshold condition, $En_i > En_{th}$.

The target UAV receives RREPs containing the HC and IL values of the respective routes. The target UAV then computes the best route R^* (route with least cost C_R , defined in (4)) by selecting among all routes that satisfy a lifetime condition (2) and an energy condition (3). The selected route is long-lasting, less-congested, and energy-sufficient. Here, the lifetime condition is,

$$RLT_R > TTL, \quad (2)$$

where TTL is the time-to-live value of the data packets. The energy condition is,

$$En_R > En_{th} + \delta_e, \quad (3)$$

For each satisfying route R , we compute the cost,

$$C_R = w_1 \left(\frac{HC_R}{HC_{min}} \right) + w_2 \left(\frac{IL_R}{IL_{min} + \alpha IL_R} \right), \quad (4)$$

where $(\cdot)_{min} = \min_{R \in X} (\cdot)_R$ and X is the set of all routes known by the target UAV that satisfy the constraints (2) and (3). The weights w_1, w_2 determine the balance between short paths (low HC) and low-interference paths (low IL), with $w_1 + w_2 = 1$; we set $w_1 = w_2 = 0.5$. To reduce the route computation delay, we only consider routes with $HC_R \leq HC_{min} + 3$. We use $\alpha = 0.3$ as the scaling factor to convert the IL cost values to a similar range as the HC cost values¹.

¹Since $HC_{min} \geq 2$, the range of $(\frac{HC_R}{HC_{min}})$ is (1, 2.5]. Similarly, since $IL_{min} \geq 2$, $(\frac{IL_R}{IL_{min} + \alpha IL_R})$ can vary from 0.77 to 3.33. However, in our simulation settings, the range of this ratio is [1, 2.5] because IL_R is generally greater than IL_{min} .

C. Pipe Formation

Since the UAV network topology changes frequently, the quality of the current active route may deteriorate over time and new, better-quality routes may become available. Ideally, the target UAV (source node) should proactively switch routes when the current route deteriorates. In practice, we accomplish this by switching to a new route when the quality of the current active route drops below a certain threshold. This proactive switching can improve throughput, reduce interruptions in data flow, and prevent packet drops due to route breaks.

Since network topology information is not centralized and no node knows the entire topology, the nodes must periodically broadcast their information via the protocol's Hello packets. As in MCA-AODV [13], the target UAV (source node) collects and builds limited network topology information around the currently used active route to form a "pipe" and enable proactive route switching. When a target is discovered, the target UAV performs route discovery and selects the best route to BS. Also, a pipe (see Figure 2) is established along the active route from the target UAV to the BS [13]. The pipe comprises the nodes along the active route (red nodes) and their 2-hop neighbors (green nodes). The topology information (including LLT, En, and IL values) of the nodes within the pipe is transmitted periodically to the source node as discussed in [13]. A pipe width of 2-hop neighbors around the active route appears to give a good trade-off between the usefulness of the neighborhood information and its incurred overhead [13]. Increasing the pipe width correspondingly increases the amount of the known network topology; while this may help identify more alternate routes, it comes at the cost of more control packets and computational overhead.

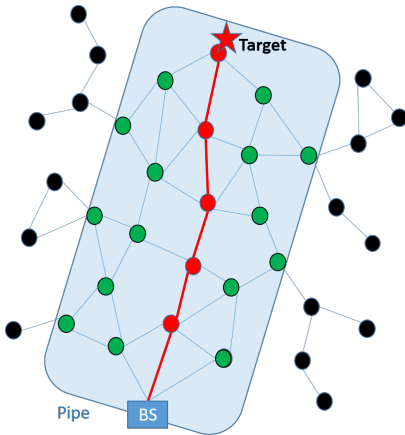


Fig. 2: Illustration of a pipe around the active route (red links) from the target UAV to BS. The pipe consists of nodes (green nodes) that are up to 2-hop from the nodes along the active route (red nodes).

D. Proactive Route Switching

Proactive route switching is triggered when the quality of the active route (R^*) degrades below a threshold, given by the conditions (2) and (3), or when a shorter alternate route becomes available in the pipe. In such a situation, the source

node initiates a breadth-first search (BFS) algorithm to explore all the available routes within the pipe to the destination node and selects the route with least cost (calculated using (4)). When the source node switches to a new active route, the existing pipe is abandoned and a new pipe is formed around the new active route. If no suitable alternate route is available, a new route discovery is triggered. By using the local pipe topology when possible, proactive route switching reduces the number of new route discoveries, and thus their overhead and delays, while minimizing the interruptions in data throughput.

IV. TOPOLOGY CONTROL

The UAVs in the network follow the BS-CAP mobility scheme for improved coverage and connectivity [12]. In this section, we discuss a topology control scheme to alter the trajectory of UAVs near the pipe region in order to maintain a robust pipe and a stable route. The proposed scheme, which combines both pipe-based routing (Section III) and topology control, is called *pipe routing with topology control* (TC-Pipe).

A. Need for Topology Control

Stable and high quality routes, along with proactively identified alternate routes in the pipe, can increase data throughput and reduce the number of route rediscoveries, thereby reducing packet loss, overhead, and delay. Although the BS-CAP mobility model tries to provide a strong node degree as well as BS connectivity, it can be difficult to achieve both fast area coverage and stable connectivity for low to medium density UAV swarms. As a result, the route between the target UAV and BS may not be stable or have sufficient quality to meet the QoS requirements. Additionally, the advantages of our pipe-based routing and proactive switching critically depend on alternate routes being available in the pipe, which is also less likely at lower densities.

The BS-CAP mobility model uses a repel pheromone, in which UAVs fly away from already-covered areas to explore the entire map, without taking into account the active route(s) being used for data communication. This can lead to sections of the pipe becoming thin, where some intermediate node(s) in the active route have very few or no neighbors. We call this effect the 'pipe thinning' problem, and illustrate it in Figure 3.

Typically, existing node mobility schemes do not consider how to facilitate a robust set of alternative routes to improve the reliability and throughput of ongoing communication to BS [14], [29], [34]. Our proposed topology control scheme uses the digital pheromone map and node-degree information of the nodes along the active route between the target UAV and BS to maintain a sufficient number of neighboring UAVs in the pipe region. Our topology control is performed by applying a pheromone mask that negates the repel pheromone (effectively acting like attract pheromone) to bring UAVs toward regions of each active route's pipe where the UAV density is low. Combined with pipe-based routing, this reduces data flow interruptions and improves throughput. It can be particularly helpful when the targets are located far from the BS (a long route length) in a network of low node density.

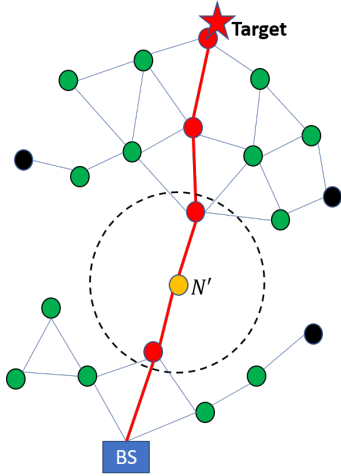


Fig. 3: Illustration of pipe thinning problem, where the node N' has no 1-hop neighbors except the upstream and downstream nodes on the active route.

B. Topology Control Scheme

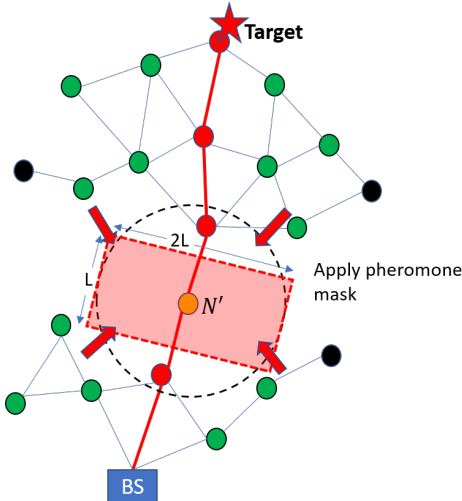


Fig. 4: Applying a pheromone mask to attract UAVs.

In Figure 3, the node N' (shown in yellow) on the active route has a low node degree, below a user-selected threshold Th , due to pipe thinning. This low degree reduces the probability of finding an alternate route in the pipe region from the target UAV to the BS. In this section, we propose a topology control scheme that uses pheromone-based mobility control to resolve the pipe thinning problem.

Since all UAVs in the network follow the BS-CAP mobility model (which is a repel pheromone-based mobility scheme), their mobility is influenced by the pheromone values of the cells [12]. The digital pheromone information is propagated to the neighbors using the Hello messages. In our updated approach, nodes on an active route apply a pheromone mask to nullify the nearby repel pheromone if their node degree is below Th . As a result, neighboring nodes that are not a part of the active route are induced to move into the region; see Figure 4 for an illustration.

Algorithm 1: Topology Control

```

1 // For an active route
2 for each node  $N'$  in active route; except BS do
3   Get  $d_{N'} = 1$ -hop node degree excluding upstream and
   downstream nodes;
4   //Node degree threshold,  $Th = 2$ 
5   if  $d_{N'} \leq Th$  then
6     // Pipe node density low in region
7     Apply pheromone mask,  $P = P_R \odot A$  from (5);
8   else
9     // Pipe node density not low in region
10    Remove pheromone mask,  $P = P_R$ ;
11  end
12 end

```

Consider a node N' located in cell (x, y) , with repel pheromone map P_R [12]. If a pheromone mask is applied by node N' , its resulting pheromone map P becomes

$$P = P_R \odot A, \quad (5)$$

where A is the pheromone mask and \odot represents an element-wise product. A is a rectangular region of dimension $2L \times L$ centered at node N' 's cell (x, y) , and oriented perpendicular to the vector connecting the upstream and downstream nodes of N' (see Figure 4). The size L is taken to be the UAV's signal transmission range, i.e., the maximum 1-hop distance between UAVs. The pheromone values of cells in A are set to zero. The mask update can be equivalently viewed as depositing an attract pheromone value in each cell equivalent to its current repel pheromone value, resulting in a net pheromone value of zero. This causes the cells under the $2L \times L$ region to attract UAVs relative to cells outside the masked region, whose repel pheromone values are generally positive.

Nodes arriving in the newly masked region provide potential alternate links and improve the robustness of the pipe region around the active route node(s). The pheromone mask is then retracted by the node(s) on the active route once its number of 1-hop neighbors exceeds Th . The topology control algorithm is described in Algorithm 1. We use the threshold $Th = 2$ in our simulations. While higher Th attracts more nodes to the 1-hop regions of the active route, doing so does not necessarily improve the routing performance and can degrade the network's area coverage at low node densities.

V. CONTROL OVERHEAD AND COMPUTATIONAL COMPLEXITY

Control Overhead: In addition to the information sent in the RREQ, RREP, RERR and Hello packets in the standard AODV protocol, each node in the proposed TC-Pipe routing scheme includes the following information in its Hello packet:

- Its UAV ID (7 bits), its current location (18 bits with 10 m resolution), next-waypoint cell (12 bits for the cell ID, assuming 60 x 60 cells of 100 m x 100 m resolution in a 6 km x 6 km area), and a local pheromone map (6-bit pheromone values in the 5 x 5 cells centered at the UAV's current cell, for 150 bits total). It also includes the hop count of the shortest route to BS (4 bits), and the pheromone mask flag/cell ID (12 bits).

- Its E_n and IL values (1 to 2 bytes).
- If the node is a 1-hop neighbor of an active node (that is participating in data packet forwarding), it broadcasts the LLT, E_n , IL, and isLinkActive values for each of its 1-hop neighbor nodes (variable size depending on neighbor density).

The destination node periodically sends the Notify_Source packet to the source node, which carries the 2-hop neighborhood information (i.e., UAV ID and their E_n , IL and LLT values) of all intermediate nodes on the route (variable size depending on 2-hop neighbor density along the route).

Computational Complexity: In the TC-Pipe routing scheme, the source node employs the BFS algorithm to discover all possible routes to the destination node within the pipe. This algorithm's worst-case time complexity is $O(TV_p^2(E_p + V_p))$, where T represents the number of route recomputations, and V_p and E_p denote the number of nodes and links within the pipe, respectively. Additionally, intermediate nodes use the Bron-Kerbosch algorithm to compute cliques within their 2-hop neighborhood. This algorithm's worst-case time complexity is $O(3^{V_p/3})$. It is worth noting that the clique computation is optional but aids in reducing control overhead.

VI. RELAY ROUTING

Our approach to mobility and routing in UAV swarms is explicitly homogeneous: each node in the network is, individually, balancing the two needs of exploration (area coverage) and communication (providing routes within the network and to the BS). A possible alternative, of course, is to assign *roles* to nodes within the network, allowing some nodes to become solely responsible for providing routing ("relays"), while others continue to explore the environment. As one example, relay UAVs might be deployed as a separate layer to provide continuous BS connectivity in a hierarchical network [39], [40].

We believe that a homogeneous approach has a number of important advantages. While a relay-based scheme prioritizes ensuring a stable communication path, by focusing on maintaining a specific route, it may create bottleneck nodes that suffer from congestion, or that can become critical points of failure to the communications structure. Moreover, these nodes may be more vulnerable to antagonistic interference (e.g., on a battlefield) [41], since differences in the nodes' behavior may indicate their current role. Finally, in low-density networks, the loss of some nodes to communication infrastructure may significantly degrade area coverage, without an obvious mechanism to trade off between the two.

In order to explore the scale of these tradeoffs to our approach, we implement a simple relay-based routing scheme (called Relay) and compare its performance with our proposed schemes. Initially, all UAVs in the network follow the BS-CAP mobility model. When a UAV finds a target, it finds the shortest route to the BS using AODV routing. The nodes along this route to BS are reassigned as relay nodes. The relay UAVs in this established route start flying in a nearly circular trajectory within or around their current grid cell to maintain the established route. Thus, a stable and permanent

route between each target UAV and BS is established for data communication. When a relay node fails, the above process is repeated to establish a new shortest route. Of course, in the presence of multiple targets, this process of selecting the shortest routes to the BS may lead to multiple active routes sharing links in common, which will result in congestion, especially at high data rates. The relay UAVs act as a separate layer from the rest of the UAVs, which continue performing area search and coverage while maintaining connectivity using the BS-CAP mobility model. Again, the more nodes are selected to act as relays, the fewer nodes are available for search area coverage, degrading the swarm's coverage performance.

VII. SIMULATION RESULTS AND DISCUSSION

A. Simulation Setup

Our experimental evaluations simulate the behavior of a swarm of 30 to 50 low SWaP fixed-wing UAVs (e.g., [42], [43]) monitoring a 6 km \times 6 km area in which fixed communication infrastructure, such as a cellular network, is not available. The aerial BS is located at the bottom center of the map, and the UAVs are launched from the vicinity of the BS. Each UAV is equipped with GPS and has a transmission range of 1 km (e.g., [4], [31], [44]). We assume a multihop topology with free space propagation (e.g., [44]). For simplicity, the UAVs are assumed to be point masses, and their mobility is limited to the X-Y plane flying at a constant altitude (typically from 200 m to 1 km above the ground [43]). UAVs perform collision avoidance through trajectory modifications [45]. To facilitate representing the pheromone map, waypoints, and coverage statistics, the area is divided into grid cells of 100 m \times 100 m each, consistent with other literature [3], [30], [31], [46]. A UAV scans the cell in which it currently resides and deposits a repel pheromone of magnitude 1. We use pheromone evaporation λ and diffusion ψ rates of 0.006 each. Table I shows the simulation parameters.

We evaluate monitoring both single and multi-target settings, across various locations; see Figure 5. The UAVs use the BS-CAP mobility model ($\beta = 1.5$) to compute their flight trajectories. All the UAVs start out from the region near the base station. If a UAV discovers a target, it becomes a "target UAV" and continuously monitors the target by circling around it. Meanwhile, other UAVs continue searching and scanning for new targets or events. The target UAV establishes a route and transmits data packets continuously to the BS.

In our simulations, we take the channel rate to be 11 Mbps and the UAV transmission range to 1 km. We consider a line-of-sight communication and ignore channel fading and noise. The packet size and TTL values are 1.5 kB and 3 s, respectively. We consider a distributed TDMA MAC protocol [47] and a large MAC queue size. Packets with the smallest time-to-expiry in the queue are pushed to the head-of-line.

In order to study the network behavior under traffic, we first simulate the UAV swarm for 1000 s, after which time all the targets have been found. Then we evaluate the throughput, routing and coverage performance for 2000 s (i.e., from 1000 to 3000 s) as the swarm monitors the targets and continues to search. We report performance metrics averaged over 30 simulation runs.

Low SWaP UAVs are prone to failure due to mechanical malfunctioning or energy depletion. To understand the impact of these issues on our routing scheme, we study the method's performance when a fraction of nodes randomly fail during the simulation time. In particular, we assign a fixed fraction of nodes (20% or 30%) a failure time during the simulation, with the time selected uniformly between 1000 and 3000s. This simulates nodes failing progressively over the course of the deployment.

TABLE I: Simulation Parameters

Parameters	Values
Simulation Time	2000 s
Map Area	6 km × 6 km
Transmission Range	1 km
Number of UAVs	30, 50
UAV Speed	20 m/s, 40 m/s
Number of Targets	1, 3
Channel Range	11 Mbps
Packet size	1.5 kB
Data Rate	1 - 3.5Mbps
TTL	3 s

B. Performance Metrics

We measure the performance of our UAV network using several routing and coverage metrics.

The *routing* properties of the network are measured by:

- *Packet Delivery Ratio (PDR)*: The ratio of total data packets received at the BS to the total data packets generated at the target UAVs. PDR is a normalized throughput and can be used to calculate other metrics such as flow throughput (PDR × data rate) and packet loss ratio (1 - PDR).
- *Route Breaks (R_b)*: The number of route breaks per data flow during the 2000 s simulation duration. Since a route break leads to new route discovery, a lower R_b value signifies more stable routes and a lower control overhead.
- *Route Up Time (R_u)*: The percentage of time a target UAV has a valid route to the BS throughout the simulation (2000 s duration). A higher value is desired as it signifies a more stable route to BS with fewer data flow interruptions.

The *coverage* properties of the network are measured by:

- *Coverage (C_v)*: The average percentage of cells in the map visited by UAVs at least once within a given duration of time; we prefer a higher C_v in a given duration of time.
- *Coverage Fairness (F)*: Represents how equally all the cells of the map are visited during a given time period, as measured by Jain's fairness index [48],

$$F = \frac{(\sum_i x_i)^2}{n \sum_i x_i^2} \quad (6)$$

where x_i is the number of scans of cell i , and n is the total number of cells in the map. A higher value of F is desired.

- *Cell Visitation Frequency (V_f)*: is the average number of times a grid cell of the area map is visited by UAVs over a given duration of time (2000 s of simulation).

Our proposed pipe routing with topology control scheme (Section IV) is referred to as 'TC-Pipe'. Pipe routing without topology control (Section III) is referred to as 'Pipe'. The 'AODV' routing scheme does not use a pipe region and topology control. The TC-Pipe, Pipe and AODV routing schemes all follow the BS-CAP mobility model. Pipe routing under the ConCov mobility scheme [31] is referred to as 'ConCov-Pipe'. Finally, the relay-based routing scheme uses the BS-CAP mobility model and is referred to as 'Relay' (see Section VI). Suffix "-20" (e.g., TC-Pipe-20, AODV-20) indicates UAVs at 20 m/s, while "-40" indicates UAVs at 40 m/s speeds.

We first discuss the routing and coverage performances of these schemes for different single and 3-targets settings with no node failure in Sections VII-C and VII-D, respectively. Next, we discuss the effect of 20% and 30% node failure on the performance of these schemes in Section VII-E. Lastly, we summarize the results in Section VII-F.

C. Performance for Single Target

We first consider the routing and coverage performance for a single flow from a target (source) to BS. The performance of a routing scheme depends on the number and location of the targets (sources). In our simulations, we considered various target locations; however, for the sake of convenience, we detail the results for three particular settings, designated C_1 , C_2 and C_3 , in which the target is located at [1.5 km, 5 km], [4 km, 4 km] and [2 km, 2 km], respectively (see Figures 5a, 5b, and 5c). Here C_1 (target located far from BS) and C_3 (target located close to BS) represent the two extremes of the map. We see that the performance of the network for other target locations (such as C_2) generally tends to fall within the performance range of the two extreme settings (C_1 and C_3).

1) *Routing Performance*:: Figures 6-9 show the routing performance (measured by average route length, PDR, route up time and number of route breaks) of different schemes (TC-Pipe, Pipe, ConCov-Pipe, AODV, and Relay) for a single data flow from a target to BS for three different target locations, represented by C_1 , C_2 and C_3 . Here, the UAV network consists of two different node densities (30 and 50 UAVs) and two node speeds (20 and 40 m/s).

Average Route Length: Figure 6 shows the average route length achieved by all the routing schemes for both densities at both speeds. We observe that the route length increases with distance between the target and BS nodes, but it does not vary noticeably when the node density and speed are changed. A shorter route length typically provides better data throughput and smaller delays. For C_1 where the target is far from the BS, our TC-Pipe scheme achieves the average route length of ≈ 8.6 , while AODV achieves ≈ 9.2 . On the other hand, for C_3 where the target is relatively close to the BS, our TC-Pipe scheme achieves the average route length of ≈ 3.8 , while AODV achieves ≈ 4.4 . Overall, the TC-Pipe scheme achieves the shortest average route length, while AODV has the longest route length, with other routing schemes (Pipe, Relay and

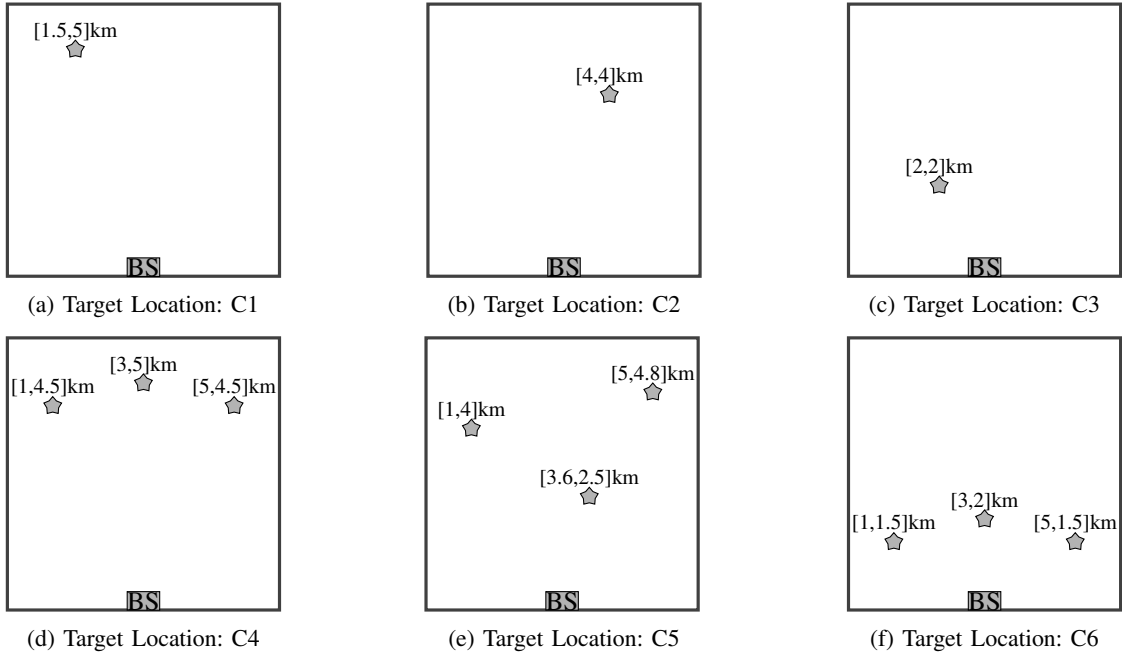


Fig. 5: The target locations in a $6 \times 6 \text{ km}^2$ map. Three different target locations are shown for a single target in (a), (b) and (c) and for a group of 3-targets in (d), (e) and (f).

ConCov-Pipe) providing average route lengths in between the two. This indicates the ability of topology control with pipe routing to establish stable, shorter routes using the pipe region.

Average PDR: Figure 7 shows the average PDR achieved by all the routing schemes for both node densities at both speeds. The average PDR achieved by a routing scheme increases as the distance between the target and BS decreases; this is because longer routes are more likely to break due to node mobility. Further, the average PDR increases for a higher density because route discovery and maintenance of pipe region is more efficient. Also, the average PDR decreases with node speed because more route breaks occur. For different network settings and target locations (C_1 , C_2 and C_3), our proposed TC-Pipe scheme achieves higher average PDR than the Pipe, AODV, and ConCov-Pipe, except the Relay scheme, as discussed below (see Figure 7).

For setting C_1 , the PDR at different data rates for both UAV densities and speeds are shown in Figures 7a and 7d. For longer routes in Figure 7a, the TC-Pipe scheme provides up to 63%, 105% and 129% increase in PDR compared to Pipe, AODV and ConCov-Pipe schemes, respectively, for 30 UAVs at 20 m/s. For higher UAV speed of 40 m/s, the TC-Pipe scheme achieves up to 52%, 113% and 100% increase in PDR compared to Pipe, AODV and ConCov-Pipe schemes, respectively. We observed similar trends for 50 nodes in Figure 7d. Even at higher UAV speeds where route breaks are more frequent, the TC-Pipe scheme achieves significant improvement in PDR compared to the Pipe and other schemes because the use of topology control in the pipe region makes the route more robust. For settings C_2 and C_3 too, TC-Pipe scheme provides higher PDR than Pipe, AODV and ConCov-Pipe, but the relative PDR improvement is reduced with the distance of the target from BS.

Further, the Pipe routing scheme performs better than AODV for both densities at both speeds for all three target locations because the use of pipe region facilitates proactive route switching instead of route rediscovery when the route quality degrades. Also, the Pipe routing scheme (which uses BS-CAP mobility model with pipe routing) performs better than ConCov-Pipe (which uses ConCov mobility model [31] with pipe routing); this demonstrates the advantage of using the BS-CAP mobility model which provides a better node degree and BS-connectivity than the ConCov model [12]. The Relay scheme achieves higher PDR performance than all other schemes, as it uses dedicated relay UAVs to establish the active route. However, as a trade-off, its coverage performance is decreased, as discussed in Section VII-C2.

Route Up (R_u): A Higher R_u value indicates that the route from target UAV to BS exists for a longer duration of time, which generally results in a more stable route providing a higher PDR. Figure 8 shows the R_u value of all the considered schemes for both node densities at both speeds. The value of R_u increases for a higher node density but decreases for a higher node speed. Here, the Relay scheme achieves the highest R_u (nearly 100%) because a stable route is established. The TC-Pipe scheme achieves the highest R_u value after the Relay scheme for both node densities at both speeds. In Figure 8b, TC-Pipe achieves R_u value of 94% and 93%, for the target location C_1 at a node density of 50 and speeds of 20 m/s and 40 m/s, respectively, compared to 87% and 83% achieved by the Pipe routing scheme. The TC-Pipe scheme's improved performance over the Pipe scheme is due to its ability to maintain a robust pipe along the active route. AODV (which uses the BS-CAP mobility model without pipe region) and ConCov-Pipe (which uses the ConCov [31] mobility model with a lower BS connectivity performance compared to the

# UAVs	Speed (m/s)	Target Location: C1					Target Location: C2					Target Location: C3				
		TC-Pipe	Pipe	AODV	ConCov-Pipe	Relay	TC-Pipe	Pipe	AODV	ConCov-Pipe	Relay	TC-Pipe	Pipe	AODV	ConCov-Pipe	Relay
30	20	8.6	8.8	9.1	9.2	8.8	7.0	7.2	7.6	7.3	7.5	3.8	4.1	4.5	4.0	4.2
	40	8.7	9.0	9.2	8.8	8.9	6.9	7.3	7.5	7.2	7.9	3.8	4.0	4.3	4.0	4.0
50	20	8.6	9.1	9.3	9.3	9.2	6.7	7.3	7.6	7.6	7.3	3.8	4.1	4.5	4.2	3.9
	40	8.5	9.1	9.3	9.1	9.3	6.7	7.3	7.5	7.4	7.1	3.7	4.0	4.3	4.1	4.0

Fig. 6: Average route length for single target locations (C_1 , C_2 , and C_3).

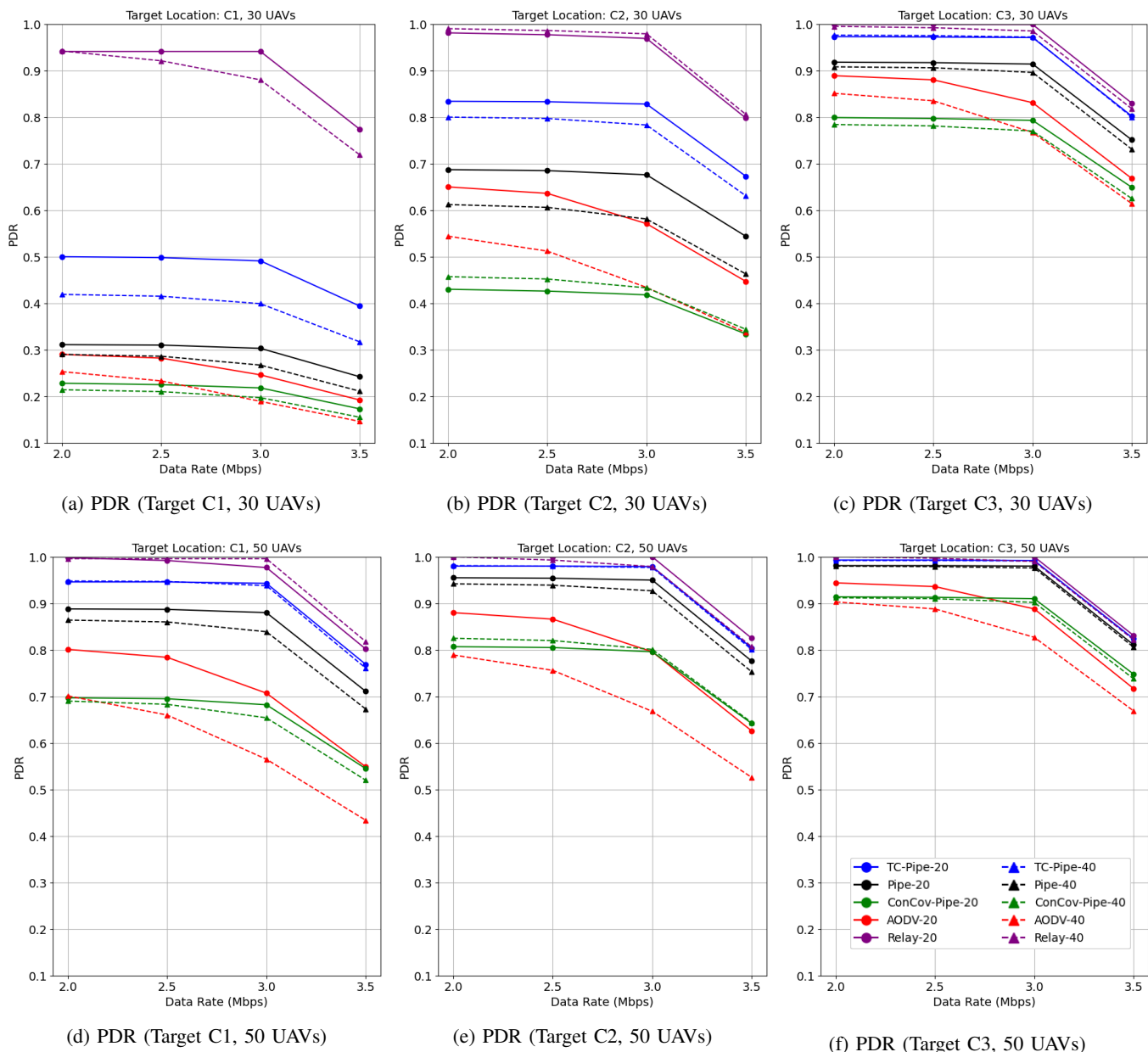


Fig. 7: Routing Performance: PDR for single target settings C_1 , C_2 and C_3 . Suffix“-20” (e.g., TC-Pipe-20, AODV-20) indicate UAVs at 20 m/s, while “-40” indicates UAVs at 40 m/s speeds.

BS-CAP mobility model [12]) provide lower R_u values. This shows that Pipe routing combined with the BS-CAP mobility model provides better routing performance (as in TC-Pipe, Pipe). A similar performance trend is observed at 30 UAV density in Figure 8a; however, the R_u performances decreases considerably, especially for longer route lengths in target setting C_1 , due to a lower node density.

Route Breaks (R_b): Figure 9 shows the number of route breaks achieved by all the routing schemes for both node densities at both speeds. Proactive route switching using the alternate route in the pipe reduces data flow interruptions and delays in pipe routing based schemes (i.e., TC-Pipe, Pipe and ConCov-Pipe). Due to better pipe robustness, the TC-Pipe scheme achieves the least route breaks (R_b) among the pipe-based schemes for both densities at both speeds and for all three target locations, reducing new route discoveries and associated control overhead. The pipe routing based schemes have far less route breaks than the AODV scheme for both densities at both speeds. For example, in target setting C_1 for 50 UAVs, TC-Pipe achieves lower R_b value of 22 at 20 m/s compared to 40 for the Pipe scheme. The ConCov-Pipe and AODV schemes yield higher R_b of 52 and 355 at 20 m/s, respectively. At UAV speed of 40 m/s, more route breaks are observed due to dynamic network topology. We find a similar performance trend across all three target locations (C_1 , C_2 and C_3) at both UAV densities at both speeds. Since the Relay scheme establishes stable routes, it experiences zero route breaks.

2) *Coverage Performance*:: Figures 10 - 12 show the coverage performance (measured by coverage vs. time, total coverage, and fairness) of different schemes (TC-Pipe, Pipe, ConCov-Pipe, and Relay) for a single data flow from a target to BS for three different target locations, represented by C_1 , C_2 and C_3 . Here, the UAV network consists of two different node densities (30 and 50 UAVs) and two node speeds (20 and 40 m/s). The performance of AODV scheme is not shown because it uses the BS-CAP mobility model with coverage performance identical to Pipe scheme.

We select the BS-CAP mobility model with $\beta = 1.5$ (for TC-Pipe, Pipe, and Relay) and ConCov mobility with $\omega = 0.5$ (for ConCov-Pipe). Among the three tuning parameter values of β and ω experimented in [12], the aforementioned middle values give a balanced coverage and connectivity trade-off performance. Also, these values give relatively similar coverage profiles (coverage vs. time curves) for the two mobility models, allowing us to compare differences in their routing performances.

The **Coverage vs. Time** plots in Figure 10 represent the total map area covered in a given time for both node densities at both speeds. The rate of area covered increases with node density as well as speed. The Relay scheme achieves a lower coverage performance compared to the Pipe and ConCov-Pipe schemes, as it reassigns some of its UAVs as relay nodes, which do not actively cover the map. This impact is more apparent at low UAV density (30 UAVs) and multiple targets (see Section VII-D2). Similarly, at low UAV density, the TC-Pipe scheme achieves a lower coverage performance because some of the UAVs are attracted to the pipe region. For setting

C_1 in Figure 11 at 30 UAVs and 20 m/s, the TC-Pipe and Relay schemes achieve C_v of $\approx 86\%$, compared to $\approx 90\%$ achieved by Pipe and ConCov schemes. Note that TC-Pipe and Relay coverage performance is comparable to Pipe and ConCov for higher node density and/or speed. For example, for 50 UAVs at 20 m/s, TC-Pipe, Pipe and ConCov achieve C_v of 99%, compared to 96% by Relay scheme.

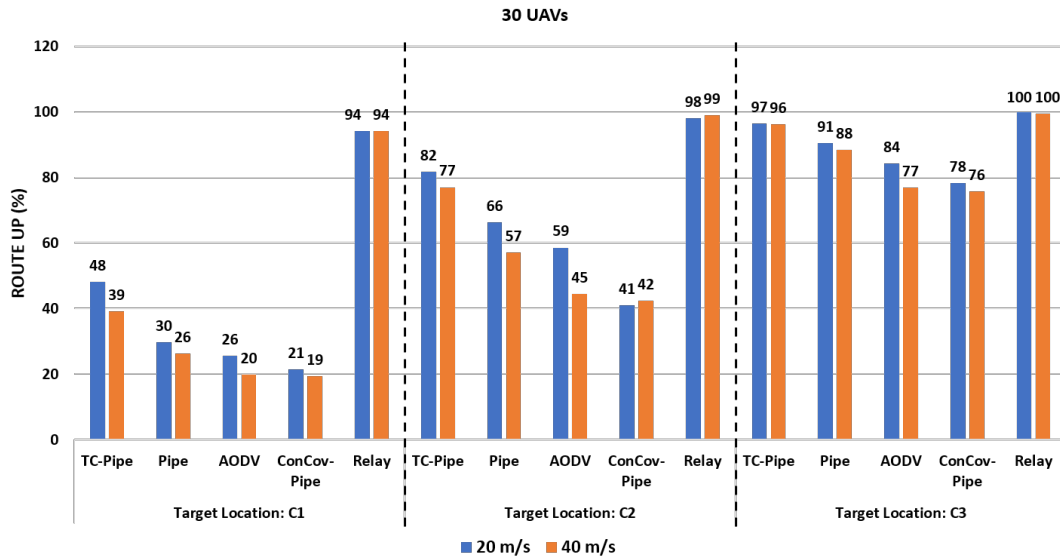
The **Fairness (F)** performance of all the schemes for both node densities at both speeds is shown in Figure 12. Each scheme achieves a higher F when the density and/or node speed increase as all the cells in the area under monitoring are visited more frequently. The TC-Pipe has slightly lower value of F than the Pipe and ConCov-Pipe schemes for 30 UAVs at both speeds for all three target locations, as some UAVs are attracted to maintain a stable pipe region. Since enough UAVs are available at node density of 50, the fairness performance of the TC-Pipe scheme is comparable to Pipe and ConCov-Pipe at both speeds. For example, in Figure 12a, for 30 UAVs in setting C_1 , TC-Pipe achieves an F of 0.67 and 0.75 at 20 m/s and 40 m/s, respectively, compared to F value around 0.71 and 0.77 (resp.) for Pipe and ConCov. In Figure 12b, for 50 UAVs in setting C_1 , TC-Pipe achieves an F of 0.87 and 0.90 at 20 m/s and 40 m/s, respectively. Meanwhile, Pipe and ConCov achieve F values of 0.88 and 0.85 at 20 m/s, and 0.92 and 0.90 at 40 m/s, respectively. The Relay scheme achieves F values of 0.83 and 0.88 for 50 UAVs at 20 m/s and 40 m/s, respectively. We further examine Relay scheme's coverage and fairness performance for three targets in Section VII-D2.

D. Performance for Three Targets

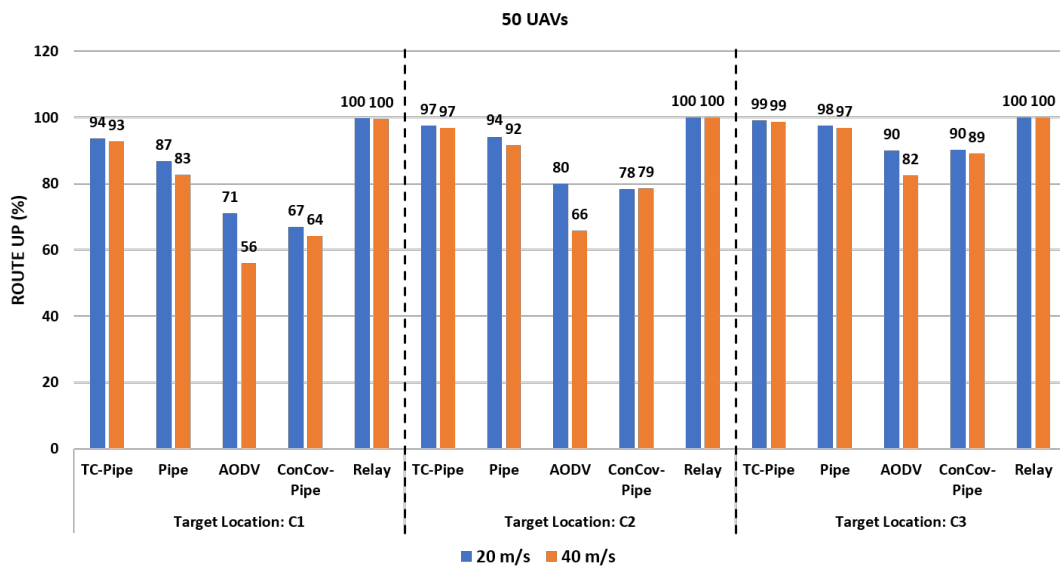
In this section, we consider the routing and coverage performance for multiple flows from three targets to the BS. In our simulations, we considered various target locations; however, for the sake of convenience, we detail the results for three particular settings, designated C_4 , C_5 and C_6 , in which the targets are located at ([1 km, 4.5 km], [3 km, 5 km], [5 km, 4.5 km]), ([1 km, 4 km], [3.6 km, 2.5 km], [5 km, 4.8 km]) and ([1 km, 1.5 km], [3 km, 2 km], [5 km, 1.5 km]), respectively (see Figures 5d, 5e and 5f). Here C_4 (targets are located far from BS) and C_6 (targets located close to BS) represent two extremes of the map. We see that the performance of the network for other target locations (such as C_5) generally tends to fall within the performance range of the two extreme settings (C_4 and C_6).

1) *Routing Performance*:: Figures 13 - 16 show the routing performance (measured by average route length, PDR, route up time and number of route breaks) of different schemes (TC-Pipe, Pipe, ConCov-Pipe, AODV, and Relay) for three data flows (one flow from each of the three targets to the BS), for three different settings of target locations, represented by C_4 , C_5 and C_6 . Here, the UAV network consists of two different node densities (30 and 50 UAVs) and two node speeds (20 and 40 m/s).

Interference and congestion may occur when multiple targets with flows to the BS exist, especially at higher data rates. The TC-Pipe and Pipe routing schemes take into consideration



(a) Route Up (30 UAVs)



(b) Route Up (50 UAVs)

Fig. 8: Routing Performance: Route Up for single target settings C_1 , C_2 and C_3 .

# UAVs	Speed (m/s)	Target Location: C1					Target Location: C2					Target Location: C3				
		TC-Pipe	Pipe	AODV	ConCov-Pipe	Relay	TC-Pipe	Pipe	AODV	ConCov-Pipe	Relay	TC-Pipe	Pipe	AODV	ConCov-Pipe	Relay
30	20	17	18	102	23	0	21	30	187	30	0	11	18	142	24	0
	40	37	40	169	32	0	43	63	314	51	0	20	39	267	42	0
50	20	22	40	355	52	0	15	30	315	45	0	7	13	166	23	0
	40	49	85	617	88	0	31	66	581	80	0	14	29	319	39	0

Fig. 9: Routing Performance: Route Breaks for single target settings C_1 , C_2 and C_3 .

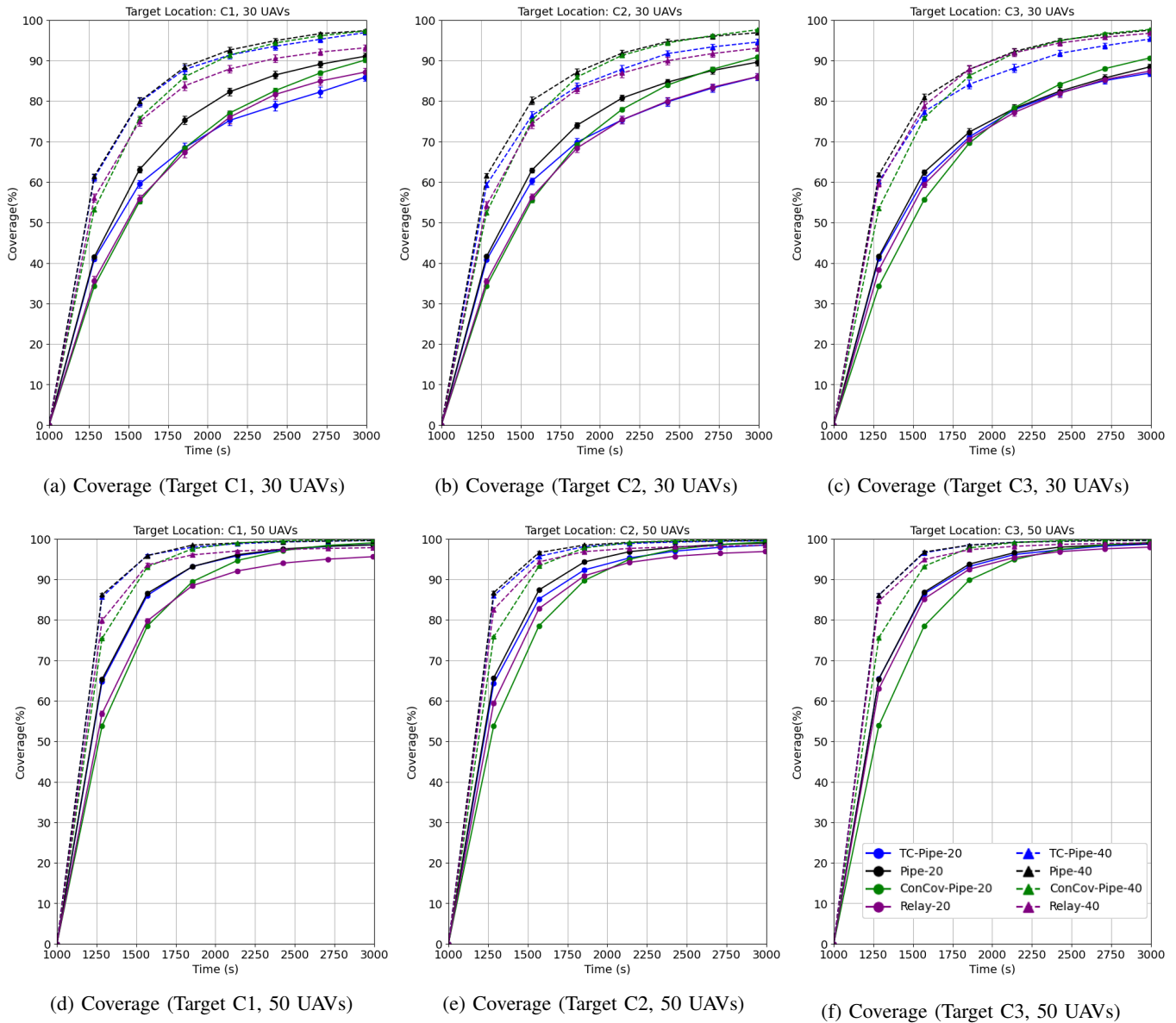
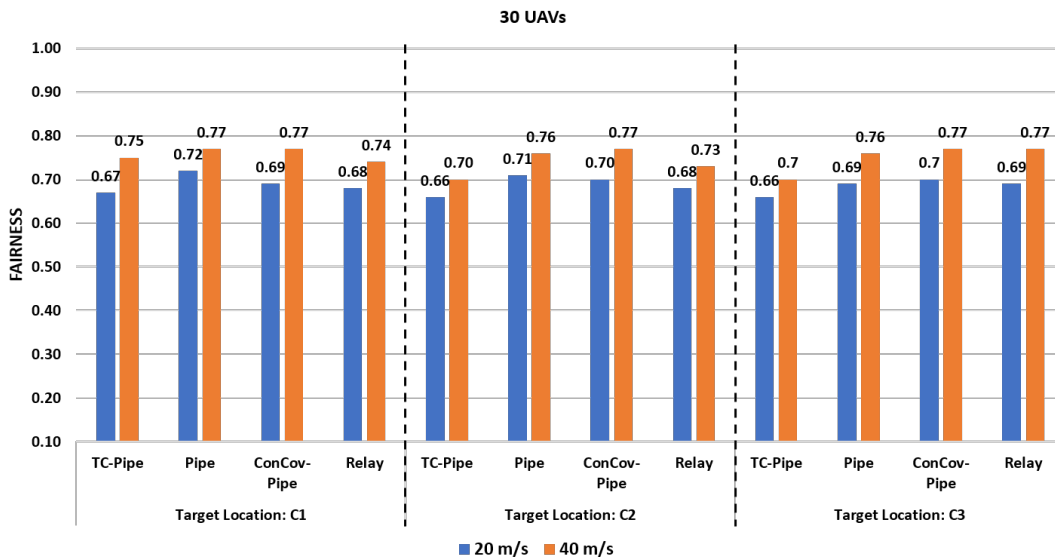


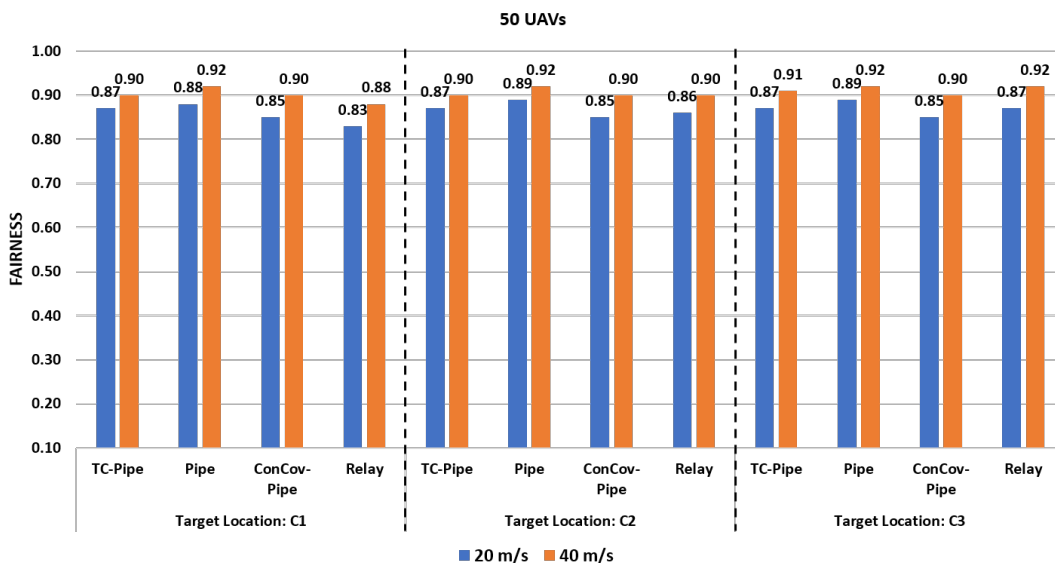
Fig. 10: Coverage vs. Time plots for single target settings C_1 , C_2 and C_3 .

# UAVs	Speed (m/s)	Target Location: C1				Target Location: C2				Target Location: C3			
		TC-Pipe	Pipe	ConCov-Pipe	Relay	TC-Pipe	Pipe	ConCov-Pipe	Relay	TC-Pipe	Pipe	ConCov-Pipe	Relay
30	20	86	91	90	87	86	90	91	86	87	88	91	87
	40	97	97	97	93	95	97	98	93	95	98	98	97
50	20	99	99	99	96	98	99	99	97	99	99	99	98
	40	100	100	100	98	100	100	100	98	100	100	100	99

Fig. 11: Coverage Performance: C_v for target single settings C_1 , C_2 and C_3 .



(a) Fairness (30 UAVs)



(b) Fairness (50 UAVs)

Fig. 12: Coverage Performance: Fairness for single target settings C_1 , C_2 and C_3 .

the congestion and interfering links between different routes when selecting an active route or when proactively switching the active routes, leading to better performance. Using the TC-Pipe scheme to maintain a robust pipe (with alternate routes) around each flow (active route) allows for selecting high-quality routes to BS with less interference and congestion. Whereas, the Pipe routing scheme (without topology control) selects less interfering or less congested routes as and when they become available in the pipe region. The AODV scheme only considers the shortest route and can therefore select routes with congested or interfering links.

Average Route Length: Figure 13 shows the average route length achieved by all the routing schemes for both densities at both speeds. We observe that the route length increases with

distance between the target and BS nodes, but it does not vary noticeably when the node density and/or speed change. A shorter route length is desired because it can provide better data throughput and smaller delays. In setting C_4 where the targets are far from BS, our TC-Pipe scheme achieves the average route length of ≈ 8.5 , while AODV achieves ≈ 9.1 . On the other hand, for C_6 where the targets are relatively close to the BS, our TC-Pipe model achieves the average route length of ≈ 4.1 , while AODV achieves ≈ 4.8 . Overall, the TC-Pipe scheme achieves the shortest average route length, while AODV has the longest route length, with other routing schemes (Pipe, Relay and ConCov-Pipe) providing average route lengths in between the two. This indicates the ability of topology control with pipe routing to establish stable, shorter

routes using the pipe region.

Average PDR: Figure 14 shows the average PDR achieved by all the routing schemes for both node densities at both speeds. The average PDR achieved by a routing scheme increases as the distance between the target and BS decreases; this is because longer routes are more likely to break due to node mobility. Further, the average PDR increases for a higher density because route discovery and maintenance of pipe region is more efficient. Also, the average PDR decreases with node speed because more route breaks occur. For different network and 3-target settings (C_4 , C_5 and C_6), our proposed TC-Pipe scheme achieves higher average PDR than the Pipe, AODV, and ConCov-Pipe schemes due to a more robust pipe which helps in selecting better quality routes (i.e., stable routes with low interference and congestion).

For target setting C_4 , the PDR at different data rates for both UAV densities and speeds are shown in Figures 14a and 14d, respectively. For longer routes, the advantage of using TC-Pipe scheme becomes more prominent. In Figure 14a, the TC-Pipe scheme achieves up to 50%, 71% and 112% increase in PDR compared to Pipe, AODV and ConCov-Pipe schemes, respectively, for 30 UAVs at 20 m/s. For higher UAV speeds of 40 m/s and 30 UAVs, the TC-Pipe scheme achieves up to 39%, 77% and 75% increase in PDR compared to Pipe, AODV and ConCov-Pipe schemes, respectively. We observed similar trends for 50 nodes in Figure 14d. Even at higher UAV speeds where route breaks are more frequent, the TC-Pipe scheme achieves significant improvement in PDR compared to the Pipe scheme because the use of topology control in the pipe region makes the route more robust. For settings C_5 and C_6 too, TC-Pipe scheme provides higher PDR than Pipe, AODV and ConCov-Pipe but the relative PDR improvement is reduced with the distance of the target from BS. For all three target settings and both UAV densities and speeds, the Pipe scheme achieves higher PDR than ConCov and AODV schemes.

For all three settings C_4 , C_5 and C_6 (for 50 UAVs) and for C_6 (for 30 UAVs), the TC-Pipe achieves better PDR than the Relay scheme for higher data rates. This is because forming shortest paths to BS without considering congestion and interference in the Relay scheme leads to poor PDR at higher data rates. Whereas, in Figure 14a, for setting C_4 with longer routes for 30 UAVs, the Relay scheme outperforms the TC-Pipe scheme. Also, the Relay scheme for three targets requires more reassigned relay UAVs to form the routes, resulting in a greater decrease in coverage performance (as discussed in Section VII-D2).

Route Up (R_u): A Higher R_u value indicates that the routes from targets UAV to BS exist for a longer duration of time, which generally provides a higher PDR. Figure 15 shows the R_u value of all the considered schemes for both node densities at both speeds. We observe that the value of R_u increases for a higher node density but decreases for a higher node speed. The Relay scheme achieves the highest R_u (nearly 100%) because a stable route is established. The TC-Pipe scheme achieves the second highest R_u value for both node densities at both speeds. In Figure 15b, TC-Pipe achieves R_u value of 95% and 92%, for the target location setting C_4 at a node density of 50 and

speeds of 20 m/s and 40 m/s, respectively, compared to 86% and 81% achieved by the Pipe routing scheme. AODV (which uses the BS-CAP mobility model without pipe region) and ConCov-Pipe (which uses the ConCov [31] mobility model with a lower BS connectivity performance compared to the BS-CAP mobility model [12]) provide lower R_u values. This shows that Pipe routing combined with the BS-CAP mobility model provides better routing performance (as in TC-Pipe and Pipe). A similar performance trend is observed at 30 UAV density in Figure 15a. For 30 UAVs, in setting C_4 where targets are located far from the BS, all schemes achieve lower R_u values (except Relay) because there are fewer UAVs in the network to maintain the routes.

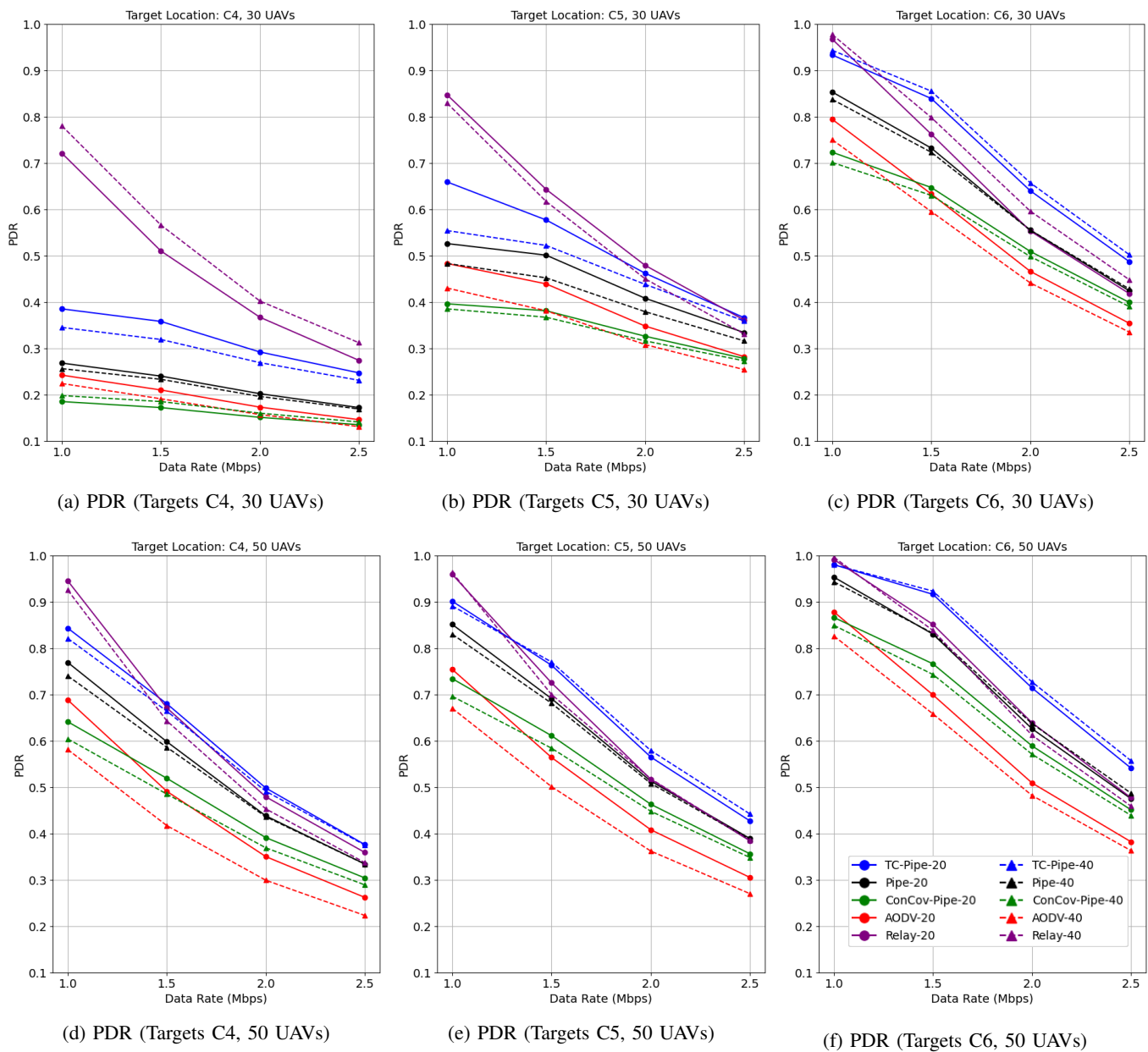
Route Breaks (R_b): Figure 16 shows the number of route breaks achieved by all the routing schemes for both UAV densities at both speeds. Proactive route switching using the alternate route in the pipe reduces data flow interruptions and delays in pipe routing based schemes (i.e., TC-Pipe, Pipe and ConCov-Pipe). Due to better pipe robustness, the TC-Pipe scheme achieves the least route breaks (R_b) among the pipe-based schemes for both densities at both speeds and for all three target location settings, reducing new route discoveries and associated control overhead. The pipe routing based schemes have far less route breaks than the AODV scheme for both densities at both speeds. In Figure 16, in setting C_4 for 50 UAVs, TC-Pipe achieves lower R_b values of 24 at 20 m/s compared to 40 in the Pipe scheme. The ConCov-Pipe and AODV schemes yield R_b of 50 and 348 at 20 m/s, respectively. At UAV speed of 40 m/s, more route breaks are observed due to dynamic network topology. We find a similar performance trend across all three target location settings (C_4 , C_5 and C_6) for both UAV densities at both speeds. Since the Relay scheme establishes stable routes, it experiences zero route breaks.

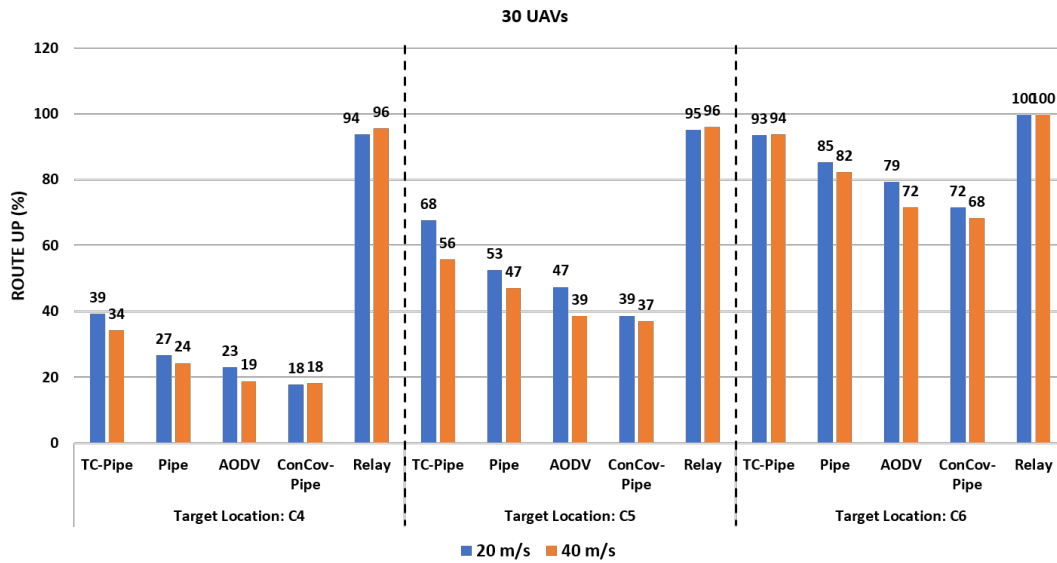
2) *Coverage Performance*:: Figures 17 - 19 show the coverage performance (measured by coverage vs. time, total coverage, and fairness) of different schemes (TC-Pipe, Pipe, ConCov-Pipe, and Relay) for three data flows from targets to BS for three different target location settings, represented by C_4 , C_5 and C_6 . Here, the UAV network consists of two different node densities (30 and 50 UAVs) at two node speeds (20 and 40 m/s). The performance of AODV scheme is not shown because it uses the BS-CAP mobility model with coverage performance identical to Pipe scheme. As explained in Section VII-C2, we select the BS-CAP mobility model with $\beta = 1.5$ (for TC-Pipe, Pipe, AODV, and Relay) and ConCov mobility model with $\omega = 0.5$ (for ConCov-Pipe).

The **Coverage vs. Time** plots in Figures 17 represent the total map area covered in a given time for both node densities at both speeds. The rate of area covered increases with node density as well as speed. The Relay scheme achieves a lower coverage performance compared to the Pipe and ConCov-Pipe schemes, as it reassigns some of its UAVs as relay nodes in the three routes to BS; these relay nodes do not actively cover the map. This impact is more apparent at low UAV density (30 UAVs). The longer the route length of these routes, the greater the number of UAVs reassigned as relay nodes, and the greater the decrease in coverage performance. This

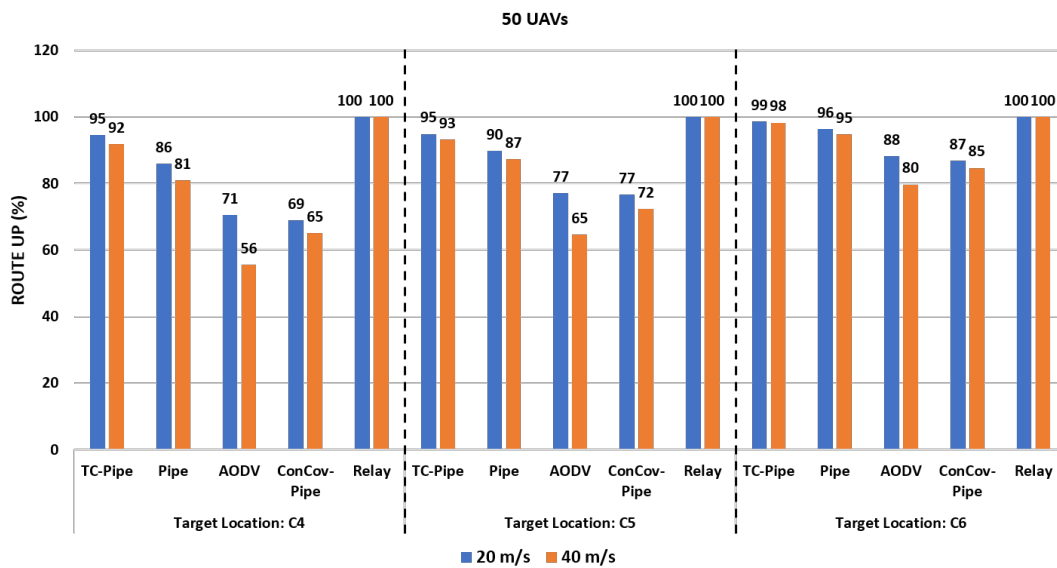
# UAVs	Speed (m/s)	Target Location: C4					Target Location: C5					Target Location: C6				
		TC-Pipe	Pipe	AODV	ConCov-Pipe	Relay	TC-Pipe	Pipe	AODV	ConCov-Pipe	Relay	TC-Pipe	Pipe	AODV	ConCov-Pipe	Relay
30	20	8.6	8.7	9.0	8.5	8.7	6.9	7.1	7.4	7.1	6.9	4.2	4.5	4.8	4.3	4.5
	40	8.5	8.7	8.9	8.5	8.8	6.8	7.1	7.4	7.0	6.8	4.1	4.5	4.7	4.3	4.6
50	20	8.4	9.0	9.3	9.0	9.3	6.8	7.2	7.5	7.4	7.1	4.0	4.5	4.8	4.6	4.7
	40	8.4	9.0	9.1	8.9	9.0	6.8	7.3	7.5	7.3	7.2	4.0	4.5	4.7	4.5	4.7

Fig. 13: Average route length for 3-target locations.

Fig. 14: Routing Performance: PDR for 3-targets settings C_4 , C_5 and C_6 .



(a) Route Up (30 UAVs)



(b) Route Up (50 UAVs)

Fig. 15: Routing Performance: Route Up for 3-targets settings C_4 , C_5 and C_6 .

# UAVs	Speed (m/s)	Target Location: C4					Target Location: C5					Target Location: C6				
		TC-Pipe	Pipe	AODV	ConCov-Pipe	Relay	TC-Pipe	Pipe	AODV	ConCov-Pipe	Relay	TC-Pipe	Pipe	AODV	ConCov-Pipe	Relay
30	20	15	16	90	18	0	18	21	123	23	0	13	20	139	25	0
	40	31	37	147	30	0	29	41	213	36	0	27	48	263	42	0
50	20	24	40	348	50	0	17	28	282	41	0	9	17	179	28	0
	40	52	90	600	90	0	38	69	521	73	0	17	40	343	47	0

Fig. 16: Routing Performance: Route Breaks for 3-targets settings C_4 , C_5 and C_6 .

is observed in Figures 17 and 18, where the Relay scheme's coverage performance is much worse in target setting C_4 than in C_6 . At low UAV density (30 UAVs), the TC-Pipe scheme achieves a slightly lower coverage performance because some of the UAVs are attracted to the pipe region to maintain its node density. However, the TC-Pipe scheme allows the UAVs participating in the route to move and cover the surrounding area, hence giving better coverage than the Relay scheme. For setting C_4 in Figure 18 at 30 UAVs and 20 m/s, the TC-Pipe and Relay schemes achieve C_v of 84% and 73%, respectively, compared to $\approx 90\%$ achieved by Pipe and ConCov schemes. TC-Pipe's coverage performance is comparable to Pipe and ConCov for higher node density, whereas Relay has a lower performance, especially for C_4 and C_5 (which correspond to medium and long route lengths). For example, for 50 UAVs at 20 m/s, TC-Pipe, Pipe and ConCov achieve C_v of $\approx 98\%$, compared to $\approx 91\%$ achieved by Relay for C_4 and C_5 .

The **Fairness** (F) performance of all the schemes for both node densities at both speeds is shown in Figure 19. Each scheme achieves a higher F when the density and/or node speed increase as all the cells in the area under monitoring are visited more frequently. F value of the TC-Pipe and Relay schemes is lower than Pipe and ConCov-Pipe schemes for 30 UAVs at both speeds for all three target location settings. In TC-Pipe, some UAVs cover the region near the pipes of three flows (due to pheromone masking), leading to a decrease in coverage fairness performance. Whereas, in Relay, more UAVs are reassigned as relay nodes to form the routes of the three flows, leading to a bigger decrease in the number of UAVs performing coverage and thus decreasing coverage fairness. For example, in Figure 19a, for 30 UAVs and setting C_4 , TC-Pipe achieves F of 0.66 and 0.74 at 20 m/s and 40 m/s, respectively, compared to F values of 0.74-0.67 and 0.77-0.76 (resp.) for Pipe and ConCov-Pipe. The Relay scheme achieves lower F values of 0.58 and 0.63 for 30 UAVs at 20 m/s and 40 m/s, respectively. Since enough UAVs are available at a density of 50 UAVs, the TC-Pipe scheme's fairness performance is comparable to Pipe and ConCov-Pipe, whereas the Relay scheme achieves lower F values (see Figure 12b).

E. Effect of Node Failures on Performance

We study the impact of node failures on the routing and coverage performance of the TC-Pipe, Pipe and Relay schemes when a fraction of nodes randomly fail during the simulation time. We consider 20% and 30% of the UAVs progressively failing during the simulation due to energy depletion and mechanical failures, and observe that the PDR and coverage performances decrease gracefully in proportion to the % UAVs failing in the network.

1) *Effect of Node Failures for Single Target*:: For single target settings (C_1 , C_2 and C_3), Figures 20 and 21 show the PDR performance of TC-Pipe, Pipe, and Relay schemes for 30 and 50 UAVs at both speeds, respectively, whereas Figures 22 and 23 show other routing and coverage metrics.

At low UAV densities and both speeds, fewer UAVs are left after node failures which are required to maintain the pipe

while also performing area coverage. For 30 UAVs, the routing performance, including PDR (see Figure 20, see highlighted column for C_2 at 3 Mbps data rate for illustration) and route up and route breaks (see Figure 22, highlighted values), of TC-Pipe and Pipe schemes decrease with increase in % node failures. The impact of node failures is more for longer route lengths. The loss of nodes reduces the rate at which the cells are covered. Since the coverage (C_v) represents the % cells covered at least once during the observation period of 2000 s, the impact of node failures on C_v is not visible; however, fairness value F decreases with increase in % node failures. For a higher node density (50 UAVs) at both speeds, the effect of node failures on routing and coverage performances of Pipe and TC-Pipe schemes is relatively low (see Figures 21 and 23, highlighted values). When a relay UAV fails in the Relay scheme, a new shortest route is re-established using AODV routing. Therefore, its routing performance remains almost unaffected by node failures; however, its coverage performance decreases considerably compared to the TC-Pipe and Pipe schemes.

2) *Effect of Node Failures for Three Targets*:: In 3-target settings (C_4 , C_5 and C_5 shown in Figure 5), a separate route is established to serve the data flow from each of three targets. Figures 24 and 25 show the PDR performance of the TC-Pipe, Pipe and Relay schemes for 30 and 50 UAVs at both speeds, respectively, whereas Figures 26 and 27 show other routing and coverage metrics.

The overall trends representing the impact of node failures on different routing and coverage metrics are similar to the single target settings discussed above. Since more nodes are required to maintain the pipe region for routes for flows from three targets, the node failures result in a relatively greater impact on the routing and coverage performances for both node densities and at both speeds in the TC-Pipe and Pipe schemes. For 30 UAVs in setting C_5 with long routes, we observe decrease in PDR, coverage and other routing metrics due to node failures (see Figures 24 and 26). For 50 UAVs at both speeds, we observe a better overall performance (due to a higher node density) but the impact of node failures is still visible, especially for a longer route length and higher % node failures (see setting C_5 in Figures 25 and 27). In the Relay scheme, the relay UAVs establish stable routes, so the PDR and other routing performance see a small decrease due to node failures. But its coverage performance becomes much worse, especially for the flows with longer route lengths. Since more UAVs are reassigned as relay nodes to form routes, fewer UAVs are available for covering the map (see C_v performance in Figure 26).

F. Summary

We see that both pipe routing and topology control contribute to maintaining a robust set of alternative routes and lead to better routing performance (higher PDR, longer route-up time, and fewer route breaks) at all settings, with TC-Pipe (which uses both) outperforming Pipe, AODV, and ConCov-Pipe. With no pipe region, AODV performs worst; the pipe region allows the other methods (TC-Pipe, Pipe, and ConCov-Pipe) to proactively switch routes within the pipe, leading to

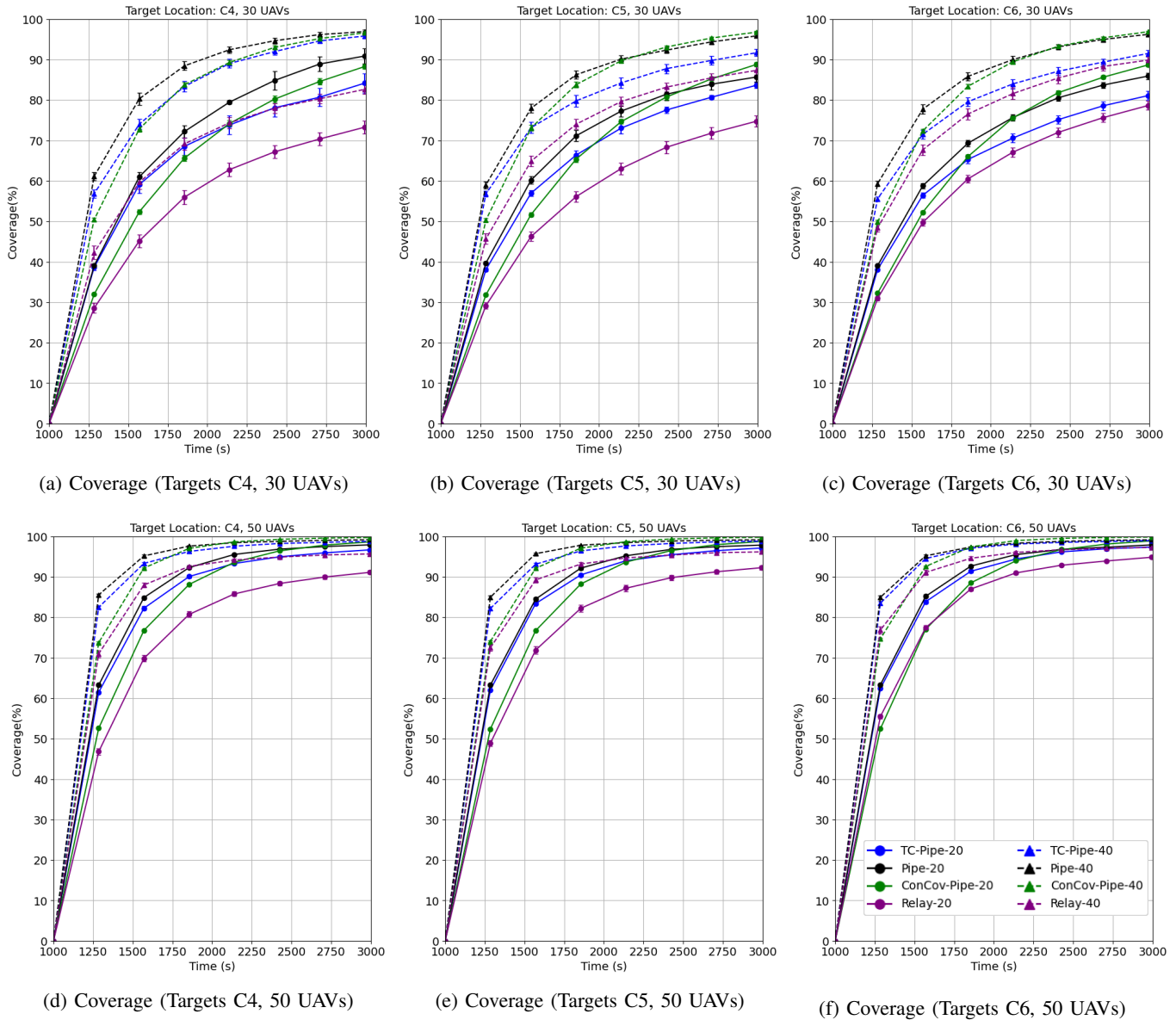
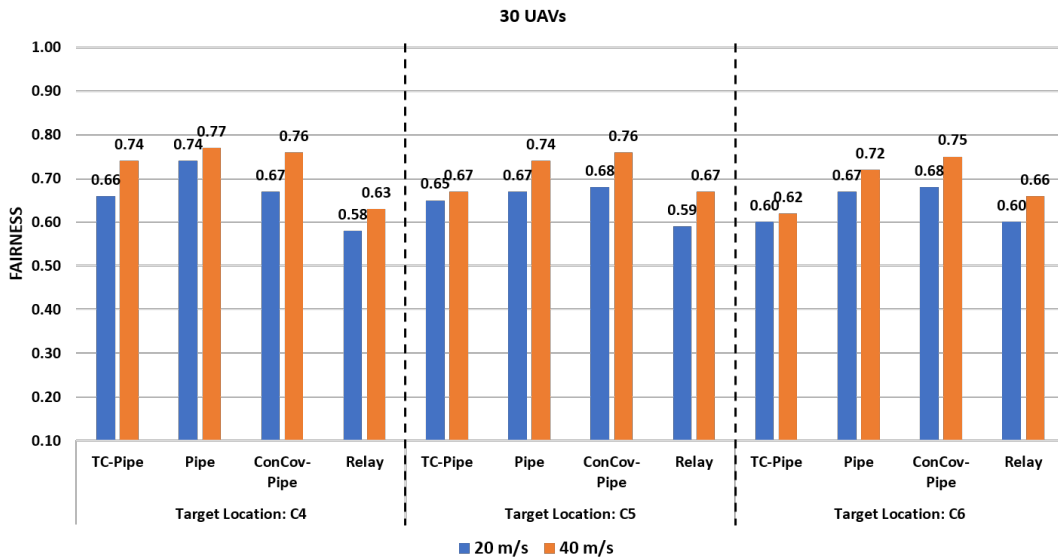


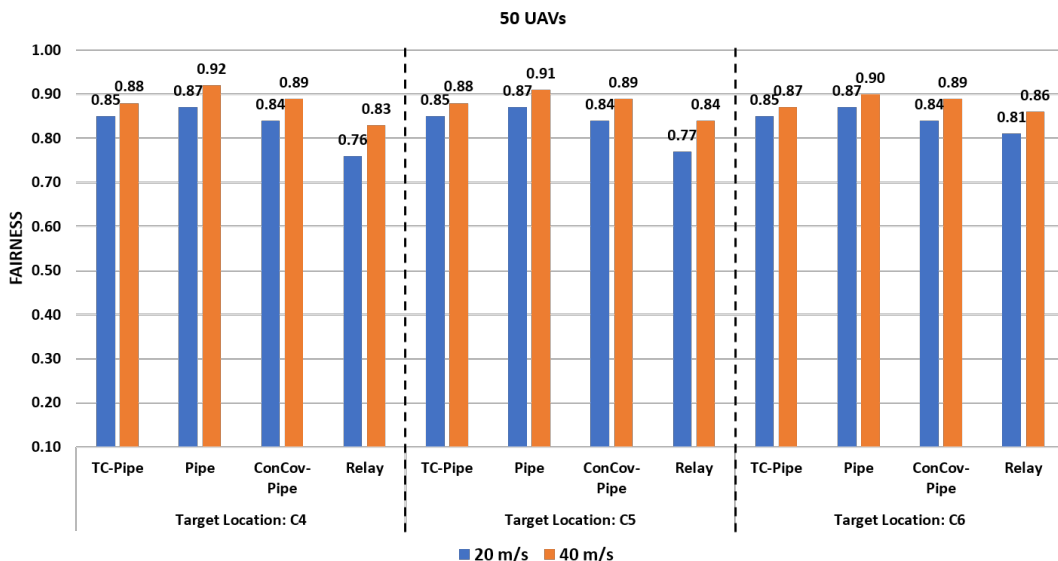
Fig. 17: Coverage vs. Time plots for 3-targets settings C_4 , C_5 and C_6 .

# UAVs	Speed (m/s)	Target Location: C4				Target Location: C5				Target Location: C6			
		TC-Pipe	Pipe	ConCov-Pipe	Relay	TC-Pipe	Pipe	ConCov-Pipe	Relay	TC-Pipe	Pipe	ConCov-Pipe	Relay
30	20	84	91	88	73	84	86	89	76	81	86	89	79
	40	96	97	97	83	92	96	97	87	92	96	97	90
50	20	97	98	99	91	97	98	99	92	97	98	99	95
	40	99	99	100	96	99	99	100	96	99	99	100	97

Fig. 18: Coverage Performance: C_v for 3-targets settings C_4 , C_5 and C_6



(a) Fairness (30 UAVs)



(b) Fairness (50 UAVs)

Fig. 19: Coverage performance: Fairness for 3-targets settings C_4 , C_5 and C_6

fewer route breaks and thus fewer route discoveries. In general, the routing and coverage performance is a trade-off [12]. TC-Pipe sees a slight decrease in coverage (C_v , F) compared to Pipe, AODV and ConCov-Pipe at lower node density (30 UAVs), but at higher density, TC-Pipe achieves comparable coverage performance with better PDR.

The Relay scheme achieves higher PDR than TC-Pipe in single target settings and some 3-targets settings (longer routes and lower data rates), because it uses dedicated relay UAVs to establish stable routes. However, it provides the worst coverage performance among the tested schemes, especially for multiple targets with long routes at low UAV density, because significantly fewer UAVs are available to perform area coverage. In both Pipe and TC-Pipe, the PDR and coverage

performances decrease gracefully in proportion to the % of UAVs failing in the network. At higher density, this decrease is less than at lower density, as there are enough UAVs to maintain a robust pipe.

VIII. CONCLUSION

We considered a decentralized, multi-hop, dynamic UAV network consisting of low SWaP UAVs, where UAVs continuously monitor the map area to find new targets and maintain routes between UAVs monitoring targets to BS for data communication. We designed a mobility, congestion, and energy-aware hybrid reactive routing protocol, called the Pipe routing (Pipe), based on the MCA-AODV [13], followed by a novel pipe routing with topology control scheme (TC-Pipe).

30 UAVs		% Node Failures	Target Location: C1			Target Location: C2			Target Location: C3		
			(Data Rate Mbps)			(Data Rate Mbps)			(Data Rate Mbps)		
			2	3	3.5	2	3	3.5	2	3	3.5
20 m/s	TC-Pipe	0	0.50	0.49	0.39	0.83	0.83	0.67	0.97	0.97	0.80
		20	0.36	0.36	0.36	0.74	0.73	0.59	0.96	0.95	0.79
		30	0.32	0.31	0.25	0.63	0.62	0.50	0.95	0.95	0.78
	Pipe	0	0.31	0.30	0.24	0.69	0.68	0.54	0.92	0.91	0.75
		20	0.25	0.24	0.19	0.54	0.53	0.42	0.88	0.87	0.72
		30	0.21	0.21	0.16	0.50	0.48	0.39	0.86	0.85	0.70
	Relay	0	0.94	0.94	0.77	0.98	0.97	0.80	1.00	1.00	0.83
		20	0.93	0.93	0.93	0.98	0.97	0.80	1.00	1.00	0.83
		30	0.92	0.91	0.74	0.95	0.94	0.78	1.00	1.00	0.83
40 m/s	TC-Pipe	0	0.42	0.40	0.32	0.80	0.78	0.63	0.98	0.97	0.80
		20	0.33	0.33	0.33	0.70	0.68	0.54	0.96	0.95	0.78
		30	0.28	0.26	0.21	0.63	0.61	0.49	0.95	0.94	0.77
	Pipe	0	0.29	0.27	0.21	0.61	0.58	0.46	0.91	0.90	0.73
		20	0.17	0.15	0.12	0.51	0.49	0.39	0.88	0.87	0.71
		30	0.16	0.14	0.11	0.44	0.41	0.33	0.86	0.85	0.69
	Relay	0	0.94	0.93	0.77	0.99	0.98	0.81	1.00	0.99	0.82
		20	0.93	0.92	0.75	0.99	0.96	0.79	0.99	0.99	0.82
		30	0.93	0.92	0.75	0.98	0.97	0.80	1.00	0.99	0.82

Fig. 20: PDR values for 30 UAVs for single-target settings C_1 , C_2 and C_3 .

50 UAVs		% Node Failures	Target Location: C1			Target Location: C2			Target Location: C3		
			(Data Rate Mbps)			(Data Rate Mbps)			(Data Rate Mbps)		
			2	3	3.5	2	3	3.5	2	3	3.5
20 m/s	TC-Pipe	0	0.95	0.94	0.77	0.98	0.98	0.80	0.99	0.99	0.82
		20	0.93	0.92	0.75	0.96	0.95	0.78	0.99	0.99	0.82
		30	0.87	0.86	0.69	0.95	0.94	0.77	0.98	0.98	0.81
	Pipe	0	0.89	0.88	0.71	0.96	0.95	0.78	0.98	0.98	0.81
		20	0.79	0.77	0.62	0.92	0.91	0.74	0.97	0.97	0.80
		30	0.71	0.69	0.55	0.90	0.89	0.72	0.97	0.97	0.80
	Relay	0	1.00	0.98	0.80	1.00	1.00	0.83	1.00	1.00	0.83
		20	1.00	0.98	0.81	1.00	0.99	0.82	1.00	1.00	0.83
		30	0.99	0.98	0.81	1.00	1.00	0.82	1.00	0.99	0.82
40 m/s	TC-Pipe	0	0.95	0.94	0.76	0.98	0.98	0.80	0.99	0.99	0.82
		20	0.89	0.87	0.70	0.97	0.96	0.78	0.99	0.98	0.81
		30	0.85	0.83	0.66	0.95	0.94	0.76	0.99	0.98	0.81
	Pipe	0	0.86	0.84	0.67	0.94	0.93	0.75	0.98	0.98	0.81
		20	0.73	0.70	0.55	0.90	0.87	0.70	0.97	0.96	0.79
		30	0.66	0.62	0.49	0.88	0.85	0.69	0.96	0.95	0.78
	Relay	0	1.00	1.00	0.82	1.00	0.98	0.81	1.00	0.99	0.82
		20	1.00	0.99	0.81	1.00	0.99	0.82	1.00	1.00	0.83
		30	1.00	0.98	0.81	1.00	1.00	0.82	1.00	0.99	0.82

Fig. 21: PDR values for 50 UAVs for single-target settings C_1 , C_2 and C_3 .

30 UAVs		% Node Failures	Target Location: C1			Target Location: C2			Target Location: C3		
			TC-Pipe	Pipe	Relay	TC-Pipe	Pipe	Relay	TC-Pipe	Pipe	Relay
20 m/s	Route Up % (R_u)	0	48	30	94	82	66	98	97	91	100
		20	36	24	93	72	52	98	95	86	100
		30	30	20	92	61	47	95	94	84	100
	Route Breaks (R_b)	0	17	18	0	21	30	0	11	18	0
		20	18	20	2	26	30	2	14	19	1
		30	20	20	3	32	33	3	17	24	1
	Coverage % (C_v)	0	86	91	87	86	90	86	87	88	87
		20	84	87	80	83	88	82	82	87	84
		30	84	89	74	84	86	75	84	86	83
	Fairness (F)	0	0.67	0.72	0.68	0.66	0.71	0.68	0.66	0.69	0.69
		20	0.65	0.68	0.62	0.62	0.68	0.65	0.61	0.67	0.66
		30	0.63	0.69	0.59	0.64	0.65	0.58	0.6	0.66	0.65
	Visitation Frequency	0	4	4	3	4	4	3	4	4	4
		20	4	4	2	4	4	3	4	4	3
		30	3	3	2	3	3	2	3	3	3
40 m/s	Route Up % (R_u)	0	39	26	94	77	57	99	96	88	100
		20	32	15	93	66	48	98	94	85	99
		30	26	14	93	60	40	98	93	83	100
	Route Breaks (R_b)	0	37	40	0	43	63	0	20	39	0
		20	32	27	2	59	60	2	29	46	1
		30	38	32	3	63	65	3	30	50	1
	Coverage % (C_v)	0	97	97	93	95	97	93	95	98	97
		20	97	97	90	94	97	92	95	97	95
		30	97	97	90	93	97	90	94	96	96
	Fairness (F)	0	0.75	0.77	0.74	0.70	0.76	0.73	0.7	0.76	0.77
		20	0.73	0.74	0.68	0.67	0.72	0.71	0.67	0.73	0.73
		30	0.72	0.72	0.68	0.66	0.73	0.69	0.64	0.72	0.73
	Visitation Frequency	0	8	8	6	8	8	6	8	8	7
		20	7	7	5	7	7	5	7	7	6
		30	7	7	4	7	7	5	7	7	6

Fig. 22: Routing and Coverage metrics: 30 UAVs for single target settings C_1 , C_2 and C_3 .

In TC-Pipe routing, the 2-hop region around the active routes (the “pipe”) is made robust using topology control; this helps to establish stable routes and improves routing performance. Both TC-Pipe and Pipe routing schemes saw fewer route breaks and better PDR than the AODV and ConCov-Pipe routing schemes. TC-Pipe achieved better routing performance than Pipe but saw a slight decrease in coverage performance at low UAV density. This is due to the inherent trade-off between connectivity and coverage performance. Though the Relay scheme establishes stable routes between the target UAVs and BS, the TC-Pipe scheme achieved better PDR for certain 3-target settings at higher data rates. In both the TC-Pipe and Pipe schemes, the PDR and coverage performances decreased gracefully in proportion to the number of failures in the network. Thus, both TC-Pipe and Pipe routing schemes are well suited for decentralized dynamic UAV networks performing target monitoring and area coverage applications.

REFERENCES

- [1] I. Martinez-Alpiste, G. Golcarenenji, Q. Wang, and J. M. Alcaraz-Calero, “Search and rescue operation using uavs: A case study,” *Expert Systems with Applications*, vol. 178, p. 114937, 2021.
- [2] E. Y. Adam, “Leveraging connectivity for coverage in drone networks for target detection,” *Balkan J. Electrical and Computer Eng.*, vol. 7, no. 3, pp. 218–225, 2019.
- [3] A. L. Alfeo, M. G. Cimino, N. De Francesco, M. Lega, and G. Vaglini, “Design and simulation of the emergent behavior of small drones swarming for distributed target localization,” *J. Computational Sci.*, vol. 29, pp. 19–33, 2018.
- [4] S. Garg, A. Ihler, E. S. Bentley, and S. Kumar, “A cross-layer, mobility, and congestion-aware routing protocol for uav networks,” *IEEE Trans. Aerospace Electronic Systems*, vol. 59, no. 4, pp. 3778–3796, 2023.
- [5] B. H. Khudayer, M. Anbar, S. M. Hanshi, and T.-C. Wan, “Efficient route discovery and link failure detection mechanisms for source routing protocol in mobile ad-hoc networks,” *IEEE Access*, vol. 8, pp. 24019–24032, 2020.
- [6] S. Garg, “An adaptive and low-complexity routing protocol for distributed airborne networks,” in *EWSN*, 2021, pp. 187–191.
- [7] C. Z. Sirmollo and M. A. Bitew, “Mobility-aware routing algorithm

50 UAVs		% Node Failures	Target Location: C1			Target Location: C2			Target Location: C3			
			TC-Pipe	Pipe	Relay	TC-Pipe	Pipe	Relay	TC-Pipe	Pipe	Relay	
20 m/s	Route Up % (R_u)	0	94	87	100	97	94	100	99	98	100	
		20	91	76	99	95	90	99	98	96	100	
		30	85	68	99	94	88	100	97	96	100	
	Route Breaks (R_b)	0	22	40	0	15	30	0	7	13	0	
		20	37	50	2	27	41	2	11	16	1	
		30	46	56	3	32	48	2	13	21	2	
	Coverage % (C_v)	0	99	99	96	98	99	97	99	99	98	
		20	97	98	94	98	97	96	98	97	97	
		30	96	97	93	96	97	95	97	97	97	
	Fairness (F)	0	0.87	0.88	0.83	0.87	0.89	0.86	0.87	0.89	0.87	
		20	0.83	0.85	0.80	0.84	0.85	0.82	0.84	0.85	0.85	
		30	0.82	0.84	0.77	0.81	0.84	0.80	0.83	0.84	0.83	
	Visitation Frequency	0	7	7	5	7	7	6	7	7	6	
		20	6	6	5	6	6	5	6	6	6	
		30	6	6	4	6	6	5	6	6	5	
	40 m/s	Route Up % (R_u)	0	93	83	100	97	92	100	99	97	100
			20	86	68	100	95	86	100	98	95	100
			30	81	61	100	93	84	100	98	94	100
Route Breaks (R_b)		0	49	85	1	31	66	0	14	29	0	
		20	77	107	2	48	91	3	22	39	1	
		30	85	107	3	60	95	3	23	45	2	
Coverage % (C_v)		0	100	100	98	100	100	98	100	100	99	
		20	99	99	98	99	99	98	99	99	99	
		30	99	99	98	99	99	98	99	99	99	
Fairness (F)		0	0.90	0.92	0.88	0.90	0.92	0.90	0.91	0.92	0.92	
		20	0.87	0.89	0.86	0.87	0.89	0.87	0.88	0.89	0.89	
		30	0.85	0.87	0.84	0.84	0.87	0.85	0.85	0.87	0.88	
Visitation Frequency		0	14	13	11	14	13	11	13	13	13	
		20	12	12	9	12	12	10	12	12	11	
		30	12	12	8	12	12	9	12	11	11	

Fig. 23: Routing and Coverage metrics: 50 UAVs for single settings C_1 , C_2 and C_3 .

- for mobile ad hoc networks,” *Wireless Communications and Mobile Computing*, vol. 2021, pp. 1–12, 2021.
- [8] M. Zhang, C. Dong, P. Yang, T. Tao, Q. Wu, and T. Q. Quek, “Adaptive routing design for flying ad hoc networks,” *IEEE Commun. Letters*, 2022.
- [9] C. Pu, “Link-quality and traffic-load aware routing for UAV ad hoc networks,” in *Int. Conf. Collaboration Internet Comput.* IEEE, 2018, pp. 71–79.
- [10] M. Song, J. Liu, and S. Yang, “A mobility prediction and delay prediction routing protocol for uav networks,” in *Int. Conf. Wireless Commun. Signal Processing.* IEEE, 2018, pp. 1–6.
- [11] M. Gharib, F. Afghah, and E. S. Bentley, “LB-OPAR: Load balanced optimized predictive and adaptive routing for cooperative UAV networks,” *Ad Hoc Networks*, vol. 132, Art. no. 102878, 2022.
- [12] S. Devaraju, A. Ihler, and S. Kumar, “A deep Q-learning based, base-station connectivity-aware, decentralized pheromone mobility model for autonomous uav networks,” *arXiv preprint arXiv:2311.16409*, 2023.
- [13] S. Garg, “Design of cross-layer mac and routing protocols for autonomous uav networks,” Ph.D. dissertation, San Diego State University, 2022.
- [14] A. H. Wheeb, R. Nordin, A. Samah, M. H. Alsharif, and M. A. Khan, “Topology-based routing protocols and mobility models for flying ad hoc networks: A contemporary review and future research directions,” *Drones*, vol. 6, no. 1, p. 9, 2021.
- [15] A. Rovira-Sugranes, A. Razi, F. Afghah, and J. Chakareski, “A review of AI-enabled routing protocols for UAV networks: Trends, challenges, and future outlook,” *Ad Hoc Netw.*, vol. 130, Art. no. 102790, 2022.
- [16] S.-W. Lee *et al.*, “An energy-aware and predictive fuzzy logic-based routing scheme in flying ad hoc networks (FANETs),” *IEEE Access*, vol. 9, pp. 129 977–130 005, 2021.
- [17] A. M. Rahmani *et al.*, “Olsr+: A new routing method based on fuzzy logic in flying ad-hoc networks (fanets),” *Veh. Commun.*, p. 100489, 2022.
- [18] C. Perkins, E. Belding-Royer, and S. Das, “Ad hoc on-demand distance vector (aodv) routing,” IETF, RFC 3561, 2003.
- [19] X. Li and J. Yan, “Lepr: Link stability estimation-based preemptive routing protocol for flying ad hoc networks,” in *IEEE Symp.Comput. Commun. IEEE.* IEEE, 2017, pp. 1079–1084.
- [20] S. Devaraju, M. Parsinia, E. S. Bentley, and S. Kumar, “A multipath local route repair scheme for bidirectional traffic in an airborne network of multibeam fdd nodes,” *IEEE Trans. Aerosp. Electron. Syst.*, vol. 58, no. 4, pp. 2983–2995, 2022.
- [21] B. H. Khudayer, M. Anbar, S. M. Hanshi, and T.-C. Wan, “Efficient route discovery and link failure detection mechanisms for source routing protocol in mobile ad-hoc networks,” *IEEE Access*, vol. 8, pp. 24 019–24 032, 2020.

30 UAVs		% Node Failures	Target Location: C4			Target Location: C5			Target Location: C6		
			Data Rate (Mbps)			Data Rate (Mbps)			Data Rate (Mbps)		
			1	1.5	2	1	1.5	2	1	1.5	2
20 m/s	TC-Pipe	0	0.39	0.36	0.29	0.66	0.58	0.46	0.93	0.84	0.64
		20	0.30	0.28	0.23	0.53	0.51	0.42	0.91	0.81	0.62
		30	0.20	0.20	0.17	0.47	0.46	0.39	0.90	0.80	0.61
	Pipe	0	0.27	0.24	0.20	0.53	0.50	0.41	0.85	0.73	0.56
		20	0.19	0.17	0.15	0.42	0.40	0.33	0.81	0.70	0.53
		30	0.19	0.18	0.16	0.42	0.41	0.34	0.79	0.67	0.52
	Relay	0	0.72	0.51	0.37	0.85	0.64	0.48	0.97	0.76	0.55
		20	0.66	0.49	0.35	0.81	0.59	0.43	0.99	0.80	0.59
		30	0.67	0.47	0.33	0.76	0.58	0.43	0.97	0.78	0.58
40 m/s	TC-Pipe	0	0.35	0.32	0.27	0.55	0.52	0.44	0.94	0.86	0.66
		20	0.25	0.23	0.20	0.51	0.48	0.41	0.91	0.82	0.63
		30	0.20	0.19	0.17	0.44	0.43	0.37	0.89	0.80	0.61
	Pipe	0	0.26	0.23	0.20	0.48	0.45	0.38	0.84	0.72	0.56
		20	0.17	0.16	0.14	0.40	0.38	0.32	0.80	0.69	0.54
		30	0.16	0.15	0.13	0.38	0.37	0.32	0.76	0.66	0.51
	Relay	0	0.78	0.57	0.40	0.83	0.62	0.45	0.98	0.80	0.60
		20	0.72	0.51	0.36	0.85	0.63	0.43	0.98	0.85	0.63
		30	0.72	0.49	0.35	0.81	0.59	0.41	0.98	0.80	0.59

Fig. 24: PDR values for 30 UAVs for 3-targets settings C_4 , C_5 and C_6 .

50 UAVs		% Node Failures	Target Location: C4			Target Location: C5			Target Location: C6		
			Data Rate (Mbps)			Data Rate (Mbps)			Data Rate (Mbps)		
			1	1.5	2	1	1.5	2	1	1.5	2
20 m/s	TC-Pipe	0	0.84	0.68	0.50	0.90	0.76	0.57	0.98	0.92	0.71
		20	0.79	0.61	0.45	0.87	0.72	0.54	0.97	0.90	0.70
		30	0.74	0.60	0.44	0.83	0.69	0.52	0.97	0.88	0.67
	Pipe	0	0.77	0.60	0.44	0.85	0.69	0.51	0.95	0.83	0.63
		20	0.71	0.56	0.41	0.79	0.65	0.49	0.93	0.80	0.61
		30	0.66	0.54	0.40	0.76	0.62	0.47	0.92	0.78	0.59
	Relay	0	0.95	0.67	0.48	0.96	0.73	0.52	0.99	0.85	0.64
		20	0.88	0.63	0.44	0.94	0.69	0.49	0.98	0.81	0.58
		30	0.88	0.61	0.44	0.93	0.68	0.49	0.99	0.85	0.63
40 m/s	TC-Pipe	0	0.82	0.66	0.49	0.89	0.77	0.58	0.98	0.92	0.73
		20	0.76	0.61	0.46	0.84	0.70	0.53	0.97	0.90	0.71
		30	0.72	0.58	0.43	0.80	0.68	0.52	0.97	0.89	0.69
	Pipe	0	0.74	0.59	0.44	0.83	0.68	0.51	0.94	0.83	0.64
		20	0.65	0.52	0.39	0.76	0.63	0.48	0.93	0.81	0.62
		30	0.58	0.47	0.36	0.71	0.60	0.46	0.92	0.80	0.61
	Relay	0	0.93	0.64	0.45	0.96	0.70	0.52	1.00	0.84	0.61
		20	0.91	0.64	0.45	0.89	0.68	0.49	0.99	0.85	0.63
		30	0.87	0.59	0.41	0.91	0.63	0.44	0.98	0.86	0.66

Fig. 25: PDR values for 50 UAVs for 3-targets settings C_4 , C_5 and C_6 .

30 UAVs		% Node Failures	Target Location: C4			Target Location: C5			Target Location: C6			
			TC-Pipe	Pipe	Relay	TC-Pipe	Pipe	Relay	TC-Pipe	Pipe	Relay	
20 m/s	Route Up % (R_u)	0	39	27	94	68	53	95	93	85	100	
		20	37	18	83	53	41	93	91	81	100	
		30	20	18	81	47	42	88	90	78	99	
	Route Breaks (R_b)	0	45	49	0	53	64	0	38	61	0	
		20	47	48	5	59	60	4	53	72	2	
		30	38	38	8	63	66	6	59	81	4	
	Coverage % (C_v)	0	84	91	73	84	86	75	81	86	79	
		20	80	88	67	80	87	66	76	85	73	
		30	84	85	59	78	85	61	73	82	68	
	Fairness (F)	0	0.66	0.74	0.58	0.65	0.67	0.59	0.60	0.67	0.60	
		20	0.63	0.69	0.54	0.60	0.68	0.49	0.55	0.64	0.56	
		30	0.64	0.66	0.48	0.58	0.64	0.48	0.53	0.62	0.52	
	Visitation Frequency	0	4	4	2	4	4	2	4	4	3	
		20	4	3	2	3	3	1	3	3	2	
		30	3	3	1	3	3	1	3	3	2	
	40 m/s	Route Up % (R_u)	0	34	24	96	56	47	96	94	82	100
			20	24	16	91	50	38	96	90	79	100
			30	19	15	91	43	37	95	88	74	100
Route Breaks (R_b)		0	94	111	0	86	124	0	81	143	0	
		20	85	87	8	99	123	4	106	164	3	
		30	86	85	9	102	123	7	120	171	5	
Coverage % (C_v)		0	96	97	83	92	96	87	92	96	90	
		20	95	96	75	90	97	78	89	94	88	
		30	95	96	71	91	95	78	86	94	83	
Fairness (F)		0	0.74	0.77	0.63	0.67	0.74	0.67	0.62	0.72	0.66	
		20	0.72	0.74	0.57	0.63	0.74	0.59	0.58	0.68	0.64	
		30	0.71	0.74	0.55	0.63	0.71	0.59	0.55	0.68	0.60	
Visitation Frequency		0	8	8	4	8	8	4	8	8	5	
		20	7	7	3	7	7	3	7	7	4	
		30	6	6	2	6	6	3	6	6	4	

Fig. 26: Routing and Coverage metrics: 30 UAVs for 3-targets settings C_4 , C_5 and C_6 .

- [22] N. Ahmad, S. Sethi, and M. Ahmed, "Cache-aware query-broadcast to improve qos of routing protocols in manets," *Wireless Pers. Commun.*, vol. 113, no. 1, pp. 481–498, 2020.
- [23] C. E. Perkins and E. M. Belding-Royer, "Quality of service for ad hoc on-demand distance vector routing," Tech. Rep., 2003.
- [24] D. Jinil Persis and T. Paul Robert, "Review of ad-hoc on-demand distance vector protocol and its swarm intelligent variants for mobile ad-hoc network," *IET Networks*, vol. 6, no. 5, pp. 87–93, 2017.
- [25] A. O. Fapojuwo, O. Salazar, and A. B. Sesay, "Performance of a qos-based multiple-route ad hoc on-demand distance vector protocol for mobile ad hoc networks," *Canadian J. Elect. Comput. Eng.*, vol. 29, no. 1/2, pp. 149–155, 2004.
- [26] S. Kumar *et al.*, "Robust on-demand multipath routing with dynamic path upgrade for delay-sensitive data over ad hoc networks," *Journal of Computer Networks and Communications*, vol. 2013, 2013.
- [27] P. Li, L. Guo, and F. Wang, "A multipath routing protocol with load balancing and energy constraining based on aomdv in ad hoc network," *Mobile Netw. Appl.*, pp. 1–10, 2019.
- [28] P. Srinivasan and P. Kamalakkannan, "Rsea-aodv: route stability and energy aware routing for mobile ad hoc networks," *Int. J. Comput. Commun.*, vol. 8, no. 6, pp. 891–900, 2013.
- [29] M. M. Alam, M. Y. Arifat, S. Moh, and J. Shen, "Topology control algorithms in multi-unmanned aerial vehicle networks: An extensive survey," *J. Network and Computer Appl.*, vol. 207, p. 103495, 2022.
- [30] S. Devaraju, A. Ihler, and S. Kumar, "A connectivity-aware pheromone mobility model for autonomous uav networks," in *2023 IEEE 20th Consumer Communications & Networking Conference (CCNC)*. IEEE, 2023, pp. 1–6.
- [31] E. Y. Adam, "Connectivity considerations for mission planning of a search and rescue drone team," *Turkish J. Electrical Engineering and Computer Sciences*, vol. 28, no. 4, pp. 2228–2243, 2020.
- [32] K. Khateri, M. Pourgholi, M. Montazeri, and L. Sabattini, "A comparison between decentralized local and global methods for connectivity maintenance of multi-robot networks," *IEEE Robotics and Automation Letters*, vol. 4, no. 2, pp. 633–640, 2019.
- [33] H. El Hammouti, M. Benjillali, B. Shihada, and M.-S. Alouini, "Learn-as-you-fly: A distributed algorithm for joint 3d placement and user association in multi-uavs networks," *IEEE Trans. Wireless Commun.*, vol. 18, no. 12, pp. 5831–5844, 2019.
- [34] N. E. H. Bahloul, S. Boudjit, M. Abdennebi, and D. E. Boubiche, "Bio-inspired on demand routing protocol for unmanned aerial vehicles," in *26th Int. Conf. on Computer Communication and Networks*. IEEE, 2017, pp. 1–6.
- [35] C. W. Reynolds, "Flocks, herds and schools: A distributed behavioral model," pp. 25–34, 1987.
- [36] A. Rahmati, S. Hosseinalipour, Y. Yapıcı, X. He, I. Güvenç, H. Dai,

50 UAVs		% Node Failures	Target Location: C4			Target Location: C5			Target Location: C6			
			TC-Pipe	Pipe	Relay	TC-Pipe	Pipe	Relay	TC-Pipe	Pipe	Relay	
20 m/s	Route Up % (R_u)	0	95	86	100	95	90	100	99	96	100	
		20	88	77	99	91	83	100	98	94	100	
		30	82	70	99	87	79	99	97	92	100	
	Route Breaks (R_b)	0	71	120	0	51	85	0	26	52	0	
		20	116	156	6	79	111	5	38	69	3	
		30	138	173	9	101	129	8	53	83	4	
	Coverage % (C_v)	0	97	98	91	97	98	92	97	98	95	
		20	95	97	89	95	97	89	96	97	94	
		30	94	96	87	95	97	89	95	96	93	
	Fairness (F)	0	0.85	0.87	0.76	0.85	0.87	0.77	0.85	0.87	0.81	
		20	0.81	0.85	0.72	0.81	0.84	0.73	0.81	0.83	0.79	
		30	0.79	0.83	0.70	0.80	0.83	0.72	0.78	0.82	0.77	
	Visitation Frequency	0	7	7	4	7	6	5	6	6	5	
		20	6	6	3	6	6	4	6	6	5	
		30	6	6	3	6	6	3	6	6	4	
	40 m/s	Route Up % (R_u)	0	92	81	100	93	87	100	98	95	100
			20	84	69	99	88	78	100	98	93	100
			30	79	60	99	84	73	99	97	92	100
Route Breaks (R_b)		0	157	271	0	113	206	0	52	121	0	
		20	225	321	8	162	243	5	77	152	3	
		30	253	322	12	187	250	9	90	162	4	
Coverage % (C_v)		0	99	99	96	99	99	96	99	99	97	
		20	98	99	94	98	99	96	99	99	97	
		30	97	99	94	98	99	95	98	99	97	
Fairness (F)		0	0.88	0.92	0.83	0.88	0.91	0.84	0.87	0.90	0.86	
		20	0.85	0.89	0.76	0.85	0.88	0.81	0.84	0.87	0.82	
		30	0.82	0.87	0.75	0.83	0.87	0.77	0.81	0.85	0.82	
Visitation Frequency		0	13	13	9	13	13	9	13	13	10	
		20	12	12	6	12	12	7	12	12	9	
		30	11	11	6	11	11	6	11	11	8	

Fig. 27: Routing and Coverage metrics: 50 UAVs for 3-targets settings C_4 , C_5 and C_6 .

- and A. Bhuyan, "Dynamic interference management for uav-assisted wireless networks," *IEEE Transactions on Wireless Communications*, vol. 21, no. 4, pp. 2637–2653, 2021.
- [37] A. Trotta, L. Montecchiari, M. D. Felice, and L. Bononi, "A gps-free flocking model for aerial mesh deployments in disaster-recovery scenarios," *IEEE Access*, vol. 8, pp. 91 558–91 573, 2020.
- [38] M. M. Alam and S. Moh, "Joint topology control and routing in a uav swarm for crowd surveillance," *Journal of Network and Computer Applications*, vol. 204, p. 103427, 2022.
- [39] E. Yanmaz, "Joint or decoupled optimization: Multi-uav path planning for search and rescue," *Ad Hoc Networks*, vol. 138, p. 103018, 2023.
- [40] J. Scherer and B. Rinner, "Short and full horizon motion planning for persistent multi-uav surveillance with energy and communication constraints," in *IEEE/RSJ Int. Conf. Intelligent Robots and Syst.* IEEE, 2017, pp. 230–235.
- [41] A. I. Hentati and L. C. Fourati, "Comprehensive survey of uavs communication networks," *Computer Standards & Interfaces*, vol. 72, p. 103451, 2020.
- [42] D. Hambling. The us navy wants swarms of thousands of small drones. <https://www.technologyreview.com/2022/10/24/1062039/us-navy-swarms-of-thousands-of-small-drones/>. Accessed Oct. 15, 2023.
- [43] Wikipedia. Aeroenvironment switchblade. https://en.wikipedia.org/wiki/AeroVironment_Switchblade. Accessed Oct. 15, 2023.
- [44] M. Alam, N. Ahmed, R. Matam, and F. A. Barbhuiya, "Ieee 802.11ah-enabled internet of drone architecture," *IEEE Internet of Things Magazine*, vol. 5, no. 1, pp. 174–178, 2022.
- [45] J. N. Yasin *et al.*, "Unmanned aerial vehicles (uavs): Collision avoidance systems and approaches," *IEEE Access*, vol. 8, pp. 105 139–105 155, 2020.
- [46] Multi-sensor payloads: Intelligence, surveillance, and reconnaissance (ISR) micro-gimbals. AeroVironment, Inc. Accessed Oct. 16, 2023. [Online]. Available: <https://www.avinc.com/uas/payloads>
- [47] S. Garg, V. S. S. Kuchipudi, E. S. Bentley, and S. Kumar, "A real-time, distributed, directional tdma mac protocol for qos-aware communication in multi-hop wireless networks," *IEEE Access*, vol. 9, pp. 26 343–26 361, 2021.
- [48] R. K. Jain, D.-M. W. Chiu, and W. R. Hawe, "A quantitative measure of fairness and discrimination," *Eastern Research Laboratory, Digital Equipment Corporation, Hudson, MA*, vol. 21, 1984.